Reduction of Unbalanced Magnetic Pull in Doubly-Fed Induction Machine

By

Obaid Aamir

Thesis submitted in fulfilment of the requirement for the degree of

Master of Engineering (Research)

School of Electrical, Mechanical and Mechatronic Systems
Faculty of Engineering and Information Technology

University of Technology Sydney (UTS)

January 2016

Certificate

I, Obaid Aamir, declare that this thesis titled, Reduction of Unbalanced Magnetic Pull in Doubly-Fed Induction Machine, and the work presented in it are my own. I confirm that:

- This work was done wholly or mainly while in candidature for a research degree at this University.
- Where any part of this thesis has been previously submitted for a degree or any other qualification at this University or any other institution, this has been clearly stated.
- Where I have consulted the published work of others, this is always clearly attributed.
- Where I have quoted from the work of others, the source is always given. With the exception of such quotations, this thesis is entirely my own work.
- I have acknowledged all main sources of help.
- Where the thesis is based on work done by myself jointly with others, I have made clear exactly what was done by others and what I have contributed myself.

Signed:
_____

Date:
_____

Acknowledgements

Firstly, I would like to express my deepest gratitude to my principle supervisor, Assoc. Prof. David Dorrell for his continuous orientation, motivations, suggestions and encouragement throughout my degree which helped me to understand and improve my knowledge in this area of research. Without him this thesis would not exist.

I would like also to thank and acknowledge my friends and colleagues for their support, help and making me feel less alone. Also, I would to take this opportunity to show my sincere grateful to University of Technology, Sydney, School of Electrical, Mechanical and Mechatronic Systems who always encouraged me.

Last but not the least; I would like to express my sincere thanks to my family for their Continuing support, being patient and faith in me throughout the last two years. Whatever I have accomplished in my academic life is because of my parents support and blessing.

Dedication

To my parents,
The reason of what I become today.
Thanks for your wonderful support.

To my sisters,
You have been my inspiration.

Abstract

This thesis reports on an investigation into the unbalanced magnetic pull (UMP) in a wound rotor induction machine due to static rotor eccentricity. Wound rotor induction machines are commonly used in wind turbines as doubly-fed induction generators (DFIGs). It is important to maintain them in good working order and operational. There can be substantial bearing wear in these machines due to their almost continuous operation, and it is important to maintain low bearing wear of these machines in order to maintain good operation. These machines can have high maintenance costs since they are located in remote locations and in the nacelle of the wind turbine. When the rotor becomes eccentric (non-centred) bearing wear is increased and the maintenance requirement increases. It has been illustrated that the UMP is higher per unit in a wound rotor induction machine compared to the cage induction machine equivalent.

In this study, a new measurement rig is developed in order to measure UMP. The methods for calculating UMP and splitting UMP and torque forces are addressed in this thesis. Furthermore, a new method for minimizing UMP is also introduced by using damper windings. Different tests and calculations are presented in this thesis. The understanding of the radial forces involved in producing UMP in a wound rotor induction machine is addressed. There is little literature on UMP in a wound rotor induction machine.

List of Symbols

$b(y,t)$	Radial flux density in air gap at point *y* and time *t* [T]
$b_n(y,t)$	Normal flux density in air gap at point *y* and time *t* [T]
$b_t(y,t)$	Tangential flux density in air gap at point *y* and time *t* [T]
b_r	Rotor slot opening [m]
b_s	Stator slot opening [m]
c	Number of turns in a coil
$e(y,t)$	Air gap electric field at point y and at time *t* [V/m]
$e_s(y,t)$	Air gap electric field due to stator current at point y and at time *t* [V/m]
f_e	Electrical frequency [Hz]
f_r	Rotor fundamental current frequency [Hz]
g	Mean air gap length when the rotor is concentric [m]
$g(x,y)$	Effective axial air gap length at point *x,y* in the air gap [m]
h	Search coil number
i_r	Rotor current [A]
$i_x(t)$	Harmonic current [A]
$j_r(y,t)$	Rotor current density at point *y* and at time *t* [A/m]
$j_s(y,t)$	Stator current density at point *y* and at time *t* [A/m]
$j_x(y,t)$	Current density at point *y* and at time *t* [A/m]
k	Inverse of average air gap radius [m]
k_r^n	Rotor slot opening factor
k_s^n	n^{th} harmonic stator slot opening factor
n	Variation in axial direction
n_s	Synchronous speed [rpm]
n_r	Mechanical speed [rpm]
p	Number of pole pairs
r	Mean air gap radius [m]
s	Motor slip [p.u.]

x	Variation in axial direction when analysing linearized machine, horizontal direction when analysing forces on axial cross section of machine, or horizontal direction of forces in UMP measuring rig [m]
y	Variation in circumferential direction when analysing linearized machine, vertical direction when analysing forces on axial cross section of machine, or axial direction of forces in UMP measuring rig [m]
x	Variation in radial direction when analysing linearized machine, or vertical direction of forces in UMP measuring rig [m]
C_w	Number of conductors in the w^{th} slot
D	Difference between centres of rotor and stator [m]
F_x	Force in x (horizontal) direction in axial cross section of machine [N]
F_y	Force in y (vertical) direction in axial cross section of machine [N]
$\bar{J}_s^n$	Stator current density coefficient of n^{th} current harmonic [A/m]
K_s	Slot opening factor
L	Axial length of the stator [m]
N_w	Number of slot at which winding is located
$\bar{N}_s^n$	n^{th} harmonic winding coefficient of stator
P	Air gap permeance [m^{-1}]
P_m	Fundamental pole pair number of machine
P_{mech}	Mechanical power [W]
R_r	Rotor resistance [Ω]
T_{mech}	Mechanical torque [Nm]
V_D	Induced Voltage [V]
∂	Degree of offset [p.u. of air gap length g]
ξ	Induced EMF [V]
μ_o	Permeability of free space
σ_n	Maxwell stress [N/m^2]
ω_m	Mechanical rotational velocity [rad/s]
Ψ_m	Air gap magnetic flux [Wb]
Ψ_r	Rotor magnetic flux [Wb]
Ψ_s	Stator magnetic flux [Wb]

Table of Contents

Acknowledgments	2
Dedication	3
Abstract	4
List of Symbol	5
List of Tables	9
List of Figures	10
Chapter: 1 Introduction	12
1.1 Background of the study	12
1.2 Research Problem	14
1.3 Objectives	15
1.4 Organization of the Thesis	15
1.5 Publication Arising Directly from the Master Research	16
Chapter 2: Literature Review and Research	17
2.1 Literature Review	17
2.2 Research Development	20
Chapter 3: Analysis of Machine	22
3.1 Machine Slip	23
3.2 Torque	23
3.3 Air Gap Length	27
3.4 Permeance	30
3.5 Unbalanced Magnetic Pull	31
3.6 Addition of 2 pole and 6 pole Search Windings	36
3.7 UMP Attenuation by Additional Windings	40
Chapter 4: Methodology and Experiments	45
4.1 Machine Settings	45
4.2 Transducers	48
4.3 Measurement of UMP	51
4.3.1 Open Circuit Test	54

4.3.2 Short Circuit Test 57
4.4 2-pole and 6-pole Search Windings 61
4.5 DC Test 73
Chapter 5: Conclusion and Future Work 74
Bibliography 75
Appendix A - Motor Specifications 81
Appendix B - 4 Pole Main Winding 83
Appendix C – 2 Pole Search Winding 84
Appendix D – 6 Pole Search Winding 85
Appendix E - Power Connections 86
Appendix F – Technical Papers Published 87

List of Tables

Table 4.1: Rotor nominally centred.

Table 4.2: 20% eccentric position of rotor.

Table 4.3: 30% eccentric position of the rotor.

Table 4.4: NDE moved 40% while DE centred.

Table 4.5: DE moved 40% while NDE centred.

Table 4.6: Short circuit and open circuit with 6 pole winding.

Table 4.7: DE 40% Eccentric

Table 4.8: NDE 40% Eccentric.

Table 4.9: NDE 20% Eccentric

Table 4.10: DE 20% Eccentric

Table 4.11: DE 5% Eccentric

Table 4.12: NDE 5% Eccentric

List of Figures

Figure 3.1: Rig including slip rings and graphite brushes.

Figure 3.2: Magnetic pole system generated by currents in the stator and rotor windings.

Figure 3.3: Equivalent circuit

Figure 3.4: Simplified Equivalent circuit

Figure 3.5: Rotor and stator positioning

Figure 3.6: DE and NDE Eccentricity

Figure 3.7: Position of coil on stator

Figure 3.8: Rotor loop representation

Figure 3.9: 2 pole and 6 pole search Winding

Figure 4.1: 4 Pole wound rotor induction machine

Figure 4.2: DE of the motor

Figure 4.3: NDE of the motor

Figure 4.4: Transducers

Figure 4.5: Analyser

Figure 4.6: Component force Sensor

Figure 4.6: Sensors position

Figure 4.7: 1st side of machine

Figure 4.8: 2nd side of machine

Figure 4.9: Test motor cofiguration

Figure 4.10: Open circuit UMP measurement results

Figure 4.11: Rotor with locking bar

Figure 4.12: Short circuit locked rotor UMP measurements

Figure 4.13: Effects of axial variation of eccentricity on the UMP

Figure 4.14: NDE moved 40% while DE centred

Figure 4.15: NDE moved 40% while DE centred

Figure 4.16: Axial variation of eccentricity.

Figure 4.17: 2 pole and 6 pole Winding

Figure 4.18: 6 Pole results with open circuit and locked rotor.

Figure 4.19: 2 Pole winding tests.

Figure 4.20: DE 40% Eccentric
Figure 4.21: NDE 40% Eccentric
Figure 4.22: NDE 20% Eccentric
Figure 4.23: DE 20% Eccentric
Figure 4.24: DE 5% Eccentric
Figure 4.25: NDE 5% Eccentric
Figure 4.26: Results of Different rotor eccentricities
Figure 4.27: Comparison of UMP with different rotor eccentricities
Figure 4.28: Comparison of voltage with different rotor eccentricities

Chapter 1: Introduction

1.1. Background of the Study

The electrical machine produces both tangential and radial electromagnetic forces on the surfaces of the rotor and stator in the air gap. The rotating torque is produced by tangential electromagnetic forces when the rotor of the machine is exactly centred and the net radial electromagnetic force on the rotor is zero. Most electrical machines work with some degree of rotor eccentricity since the axes of the stator and rotor rarely correspond to each other. This can be due to wear of bearings, bending in the rotor shalt, tolerances in manufacturing and many other manufacturing influences.

The imbalance in the electromagnetic forces on the stator and the rotor produces a net radial force on the rotor if the stator bore axis does not match with the axis of the rotor. There will obviously be an equal and opposite force on the stator. The electromagnetic force acting on the rotor depends on the degree of movement of the rotor axis away from the stator axis. This is called rotor eccentricity. The total force is the sum of the forces acting on the rotor surface around the air gap and this varies in an irregular manner when there is a net force. This net force pulls the rotor even further out of alignment and is known as Unbalanced Magnetic Pull (UMP). Further increase in eccentricity and UMP may cause damages to the machine in motion.

Rotor eccentricity is expressed in different ways, but usually it is defined in terms of either static eccentricity or dynamic eccentricity. If the radial motion of eccentric rotor remains stationary with the stator, and the rotor still rotates on its own axis, it is called static eccentricity and results in a steady pull force towards the point of minimum air gap. When the rotor still rotates on stator centre but is not rotating on its own axis this is said to be dynamic eccentricity, and results in the rotating UMP force vector. Static eccentricity can be caused by a misaligned or worn bearing whilst dynamic eccentricity can be caused by a bent shaft. Both conditions can be caused by general manufacturing and assembly variations and can exist together. Most studies that attempt to model this problem assume that the eccentricity is constant down the axial length of the machine but this is an approximation to the real situation and axial variation of eccentricity is investigated in this study.

Normal analysis techniques usually ignore the tangential force on the rotor surface and only consider the normal force. The analyses then usually assume the normal force is produced only

by the flux crossing the air gap in a radial direction. If a harmonic air gap flux wave technique is used to analyse the UMP then it can be shown that the UMP is produces by two flux waves existing in the air gap which have pole-pairs differing by one. Hence, for a 4-pole machine, as investigated here, rotor eccentricity produces a 2-pole flux wave and a 6-pole flux wave, and these to flux waves interact with the 4-pole main flux to produce UMP.

Along with UMP in the machine, there are different factors which influence in the mechanical wear and aging in an electrical machine, speed and performance. Rotor eccentricity can produce uneven current distribution in parallel windings in a machine and these can lead to localized hot spots in some coils with winding degradation and failure.

In recent years, induction machines have been used in wind turbine systems as generators. There are two types of induction machine: (a) squirrel cage induction machines and (b) wound rotor induction machines. Both machines have stator structures which similar to alternating current synchronous generators, and these consist of a hollow cylinder of laminated sheet steel with punched longitudinal slots. A Magneto-Motive Force (MMF) wave is produced in the air gap when a polyphase winding (invariably a 3-phase winding in larger machines) is placed in the slots and connected to a suitable ac supply.

A wound rotor induction machines rotor is similar to that of squirrel cage induction machine. The only difference is that short circuited squirrel cage winding is replaced by a three phase insulated winding in a similar manner to the stator. The winding of the rotor is usually wye connected and accessed via external slip rings on the shaft. Traditionally, the purpose of slip rings is to provide external additional resistance to each phase of the rotor to improve the starting characteristic of the motor. There were also ways to recover the energy dissipated in the resistors via schemes called slip-energy recovery schemes. However, the concept of the slip-energy recovery has now been extended to allow generation at sub-synchronous speeds by injecting power into the rotor at slip frequency via the rings, with the power coming from the grid via back-to-back 3-phase inverters. At super-synchronous speeds power exits the rotor via the slip rings. In this way the machine can now be used as a generator with wide speed range and a partially rated inverters system, with most of the power still flowing from the grid-connected stator windings. This had led to a renaissance in the use of wound rotor induction machines.

However, Dorrell [56] did show that wound rotor machines do have higher UMP compared to their cage rotor equivalents and given the remote locations of many wind turbines and difficult

access to the generator at the top of the turbine tower in a nacelle, it is highly advantageous to be able to calculate the UMP in a machine and also search for methods to minimize the UMP. Any calculation methods needs to be validated experimentally. To this end, the main aim of this study was to set up a test bed for the measurement of UMP in a wound field induction machine and initiate the study of the use of auxiliary windings for reducing UMP.

1.2. Research Problem

A rotating moment about the axis of the induction machine is created if the rotor of the machine is mechanically centred within the stator and slotting effects are neglected. A net radial force created due to change in position of the rotor at this unstable point pulls the rotor further out of alignment; this force is known as unbalanced magnetic pull (UMP).

This thesis is aimed at studying of UMP, and also the reduction of the UMP, in a wound rotor induction machine. When the rotor position in a stator is not in centre of the stator bore or there is the presence of some other asymmetric rotational magnetic flux in the air gap of a machine then there is a cause of UMP in the machine. UMP increases wear on bearings and plays a role in shortening the life of a machine, or reducing maintenance periods of the machine. In extreme cases it can cause failures. Moreover it also affects the support structures of rotor and stator since it can also lead to vibration, especially when the eccentricity is of the dynamic form where the force vector is rotating. Usually UMP is the effect of rotor eccentricity; either static eccentricity and dynamic eccentricity or possibly a function of both. The process of assembling and manufacturing motor may result in air gap eccentricity. The manufacturing tolerances of the stator bore and centring of the bearings can cause static eccentricity as already stated. The wearing and incorrect positioning of bearings results in excessive UMP. When the rotor moves its position from the stator centre but still rotates on stator centre, i.e., it does not rotate on its own centre, is said to be dynamic eccentricity. These both eccentricities can exist at the same time. The normal causes of the dynamic eccentricity is a bent shaft, manufacturing tolerances and incorrect manufacturing. Incorrect manufacture is less likely to produce this situation. Rotor whirl at a critical speed can also produce dynamic eccentricity although this may not be synchronous with the rotor [68]. The non-centred position of rotor in a stator or the presence of unsymmetrical magnetic flux in the air gap causes unbalanced magnetic pull (UMP) in a machine. This affects the motor in terms of maintaining good performance and causes bearing wear.

1.3. Objectives

Induction machines are widely used as generators in wind turbines as already discussed. It is important to maintain good operation and low bearing wear of these machines. The radial forces and vibrational behaviour of the rotor results in unbalanced magnetic pull in the machine and these are key factors in producing excessive bearing wearing and required increased maintenance. The main objective of this research is to calculate and measure the unbalanced magnetic pull in the machine caused by static rotor eccentricity (which is probably the most common form of eccentricity) and to develop methods to minimize the UMP. In the case of static eccentricity the radial air gap length is fixed and is caused by the incorrect positioning of rotor or stator at the time of manufacturing or by the ovality of stator core. The occurrence of static eccentricity is because of rotor centric axis is displaced from the stator axis but remains stationary with respect to the stator. The permeance harmonic method is used to analytically calculate the UMP.

This research put forwards the methodology to reduce UMP in machine by introducing damper windings in the machine. Moreover, the method of positioning rotor in different eccentricities is also proposed to observe the minimization effect of UMP in the machine.

The main work in this thesis concerns the UMP measurement rig however analysis is put forward to enable further study elsewhere and the use of UMP damper windings are discussed. The machine studied here requires rewinding in order to have damper windings with sufficient MMF to control the UMP and was thus deemed to be outside the scope of the project in terms of experimental study. However, pole-specific search coils were fitted in order to detect rotor eccentricity and this is reported on.

1.4. Organization of the Thesis

This thesis is structured as follows:

Chapter One: This chapter provide an introduction to the research and the main objectives behind this research.

Chapter Two: A literature survey of UMP in rotating electrical machines is presented. This chapter aims to review UMP analysis and measurement methods.

Chapter Three: An analysis method for calculation of the machine UMP is presented in here. The determination of machine slip, torque, permanence and air gap length is presented in this chapter. Furthermore, the method of coupling impedance is used to calculate the UMP using additional pole windings in the machine.

Chapter Four: This chapter provides a methodology for the measurement of the UMP and also proposed a method for minimizing UMP in a wound rotor induction machine. The results obtained from the proposed methods are discussed here. A study for the detection of rotor eccentricity is also put forward in this chapter and initial results are given.

Chapter Five: This chapter presents a conclusion and summary of the thesis and some potential future work for this research.

1.5. Publication Arising Directly from the Master Research

This work has contributed to three technical papers:

1. D. G. Dorrell, and O. Kayani. "Measurement and Calculation of Unbalanced Magnetic Pull in Wound Rotor Induction Machine." *Trans. on Magnetics, IEEE* Vol. 50, no. 11, Nov. 2014

   Abstract: This paper addresses the measurement and calculation of unbalanced magnetic pull (UMP) in a wound rotor induction machine. A new rig for measuring UMP is presented. To the authors' knowledge this type of rig has not been tested before. The paper details the force calculation method and a method for splitting the UMP and torque. Wound rotor induction machines are now popular as generators in wind turbines. It is important to maintain good operation and low bearing wear, and the UMP in these machines is higher than the cage-rotor equivalent because the cage damps the UMP. There is little literature on the UMP in a wound rotor machine.

2. D. G. Dorrell, O. Kayani and A. Salah, "The detection and suppression of Unbalanced Magnetic Pull in Wound Rotor Induction Motors Using Pole-Specific Search Coils and Auxiliary Windings," to be presented at *IEEE ECCE Conference*, Montreal, Sept 2015.

   Abstract: In large induction machines (such as large cage induction motor pumps in the petro-chemical industry and cage or wound-rotor induction generators in wind turbines) reliability and longevity is advantageous. This is particularly relevant to wind turbine generators which can be inaccessible. There will be some degree of tolerance and wear that will lead to low-level rotor eccentricity. For a pm-pole pair machine there will be $p_m \pm 1$ pole pair flux waves set up by the eccentricity which will generate unbalanced magnetic pull (UMP), as well as additional higher space harmonics. This paper addresses the use of stator damper windings to reduce the side-band flux waves and hence attenuate the UMP. Examples are put forward in terms of a 10 pole cage-rotor machine with static or dynamic rotor eccentricity and then extended to use a 4 pole machine wound-rotor machine. A tested analytical model is developed to include

these damper windings and the wound rotor; they are shown to reduce the UMP, particularly in a wound-rotor machine. The simulations here are in terms of a wound-rotor machine but this can be extended for DFIG operation.

Chapter 2: Literature Review and Research

2.1. Literature Review

The research on unbalanced magnetic pull emerged in 1918 through a publication on the work carried out to determine UMP [1]. Rosenberg worked on “critical induction” in machines and tried to investigate whether it results in higher unbalanced magnetic pull in machines than any other induction machines [2]. He also tried to evaluate UMP by calculating the air gap flux imbalance using B-H curves. His paper also describes UMP effect as a basis on the critical speed in machine designs.

Electromagnetic forces due to rotor eccentricity have been extensively studied using analytical methods. UMP in synchronous and induction machines due to static eccentricity was studied analytically by Robinson 1943 [3]. A set of linear equations was presented to calculate the UMP for eccentricities up to 10 % of the average air gap length. Crawford puts forward the consideration of slot combinations, windings, rotor assemblies, critical speeds, and vibration problems. The methods to calculate the vibratory forces and acoustic noise have all been investigated in relation to air gap eccentricity and unbalanced magnetic pull [4].

A study of UMP was performed on machines having series windings in conditions of light load by Covo [5]. He tried to understand the fluctuating behaviour of eccentric forces on machines and calculated UMP more precisely.

In [6], Summers put forward on extensive study on 2-pole A.C machines and theorized UMP using rotating field components. He came up with a theory that twice-line-frequency vibrations are produced with static eccentricity caused by deformations in motor and twice-running frequency vibrations are produced due to imbalances and irregularities in rotor causing dynamic UMP. The twice-slip-frequency beat vibrations are generated as a reaction of static and dynamic eccentricity UMP in these 2-pole A.C machines. The work was followed by Robinson [7], who found the existence of line frequency vibrations using mechanical resonance. Further work was carried out by Jordan [8] in 1967 and Rai [9] in 1974. Evidence of rotor eccentricity causing noise in a machine was documented by Ellison and Moore [10]. The UMP can be reduced by the use of parallel windings and this was modelled in [3], [11], and [12].

The dependence of the machine pole number on the damping of the rotating magnetic field in a rotor cage were observed by Schuisky [13] in 1971. The air gap permeance modulates the MMF wave which consists of sinusoidal wave series and a constant component. This work explains the presence of the magnetic field harmonics in a machine. The occurrence of homopolar flux was identified in two pole motors. This flux crosses the air gap and returns through the bearings, shaft and casing [14]. In [15] a study did contrast the variation between a two pole machine and a machine with more than two poles and concluded that the two pole motor was a special case. [16] – [18] further studied two pole induction motors and investigated UMP and homopolar flux in them.

Belmans [19] stated that there occurs a linkage between homopolar flux and UMP in a machine with static eccentricity. His work showed that a UMP with twice supply frequency is produced by the generation of homopolar flux.

The emission of acoustic noise as a result of radial vibrating field theory in a two pole single phase induction motor was studied by [20]. This presented the effects on the vibration and noise caused by static and dynamic eccentricities due to homopolar flux in an induction motor. It was noticed that a number of low frequency radial forces in a motor were caused by homopolar flux. [21] reported on further analysis of the noise and vibrations in machines. [22] puts forward work on UMP which is applicable to different pole number machines.

In 1983 [23] , Williamson came up with an analysis technique based on the study of machines using generalised harmonic analysis [23]. This method was earlier used to identify rotor cage end-rings, inter-rings and stator windings fault by Williamsons and Smith in 1982 [24]. Williamson and Mirzoin in 1985 [25], Williamson and Abdel-Magied in 1987 [26] and Williamson and Adams in 1989 [27] also used this idea in their research to identify faults in a motor. This method determines of coupling impedences, which links various circuits with current flowing to any windings with applied voltages in the machines.

Swan presented a technique of conformal transformation to study induction motors in 1963 [28]. The method of generalised harmonic analysis along with the method of conformal transformation were used on induction motors with parallel stator windings to compute UMP by Dorrell and Smith in 1994 [29]. An approach to the study of UMP in a machine using earlier approaches was presented by Smith and Dorrell in 1996 [30]. The divergence in the direction of UMP from the direction of rotor eccentricity due to parallel stator windings was noted in their studies together with the generation of twice supply frequency vibration.

A model for the magnetic fields in the air gap of an electrical machine using permeance harmonic analysis was presented by Heller and Joke in 1969 [31]. Further work was carried out by Vandeuelde and Melkebeet in 1994 [32] to identify the integrated effects of rotor saturation, eccentricity and slotting in the analysis of the magnetic field using permeance harmonic analysis. A procedure to investigate the EMFs in induction machines with the rotor rotating at variable frequencies using the permeance harmonic theory was developed by Früchtenicht *et al*. in 1982 [33]. Winding variables were utilized to model the winding distribution in order to calculate the MMF in induction machines by Stavrou and Penmare in 2001 [34]. Berman, 1993 [35], studied the effects of connection equalization in induction machine stator windings with dynamic and static rotor eccentricities using permeance harmonic analysis. They proposed an effective method to calculate MMF.

To observe and study the currents and inductances in a machine, WFA (Winding Function Approach) has been used in several different publications [36]-[39]. WFA was first presented and used in [40]. The linear behaviour with increasing MMF in the motor slots and the effects of rotor bar skewing was studied in [41]. He also investigated the effect on machine inductance. Further investigations on machines using this approach were developed by [42]. A modified approach was developed in [42] and named MWFA (Modified Winding Function Approach). Further work was conducted in [43] to [46]. Using machines with dynamic eccentricity, another study of the MMF in the slots and rotor skew was published in [47]. Bassio *et al.* 2004 gave a new method for the study of machines with dynamic and static eccentricity in [48].

UMP was noted as being linear with rotor eccentricity in switched reluctance machine by Garrigan *et al.* [49]. However, a reduction in UMP was also noted when there was a reduction in air gap in the saturation region. This is because when the air gap is small, the steel saturates, so any additional increase in flux is difficult. Their study concluded that the windings, connected in parallel played a vital role in reduction of UMP in the machine.

Brushless permanent magnet motors with levitation force and main windings were investigated using rotating field theory by Dorrell *et al.* (2003) [50]. They put forward a mathematical method to calculate the radial force using the theory on eccentric permanent magnet rotors. Their results matched well the simulation results. A conformal transformation technique presented by Swann 1963 [28] was utilized by Li *et al.* [51] in 2007 for a permanent magnet machine in order to determine the magnetic field in the air gap.

An increase in the UMP when a cage machine was loaded from no load was observed by Dorrell in 1995, and Dorrell in 1996 [52][53]. The machine has static eccentricity. The calculated and measured results matched well. Work was carried out on UMP reduction by Dorrell 1999 in [54] where the factors of parallel stator, rotor windings connections and variable frequency operations where investigated. Non uniform eccentricity, where the eccentricity changes down the axial length of the machine, was studies uning rotating field-theory by Dorrell 2000 [55].

An analysis was developed to calculate UMP using stator currents, rotor currents, damper currents and flux waves in [56]. A wound rotor model was developed which included stator damper windings. The assumption was made that the damper windings had little effect on torque, even when there was rotor eccentricity. It was shown that the damper windings had little effect in a cage induction motor but it was shown that they are more effective in wound rotor induction machines. A number of recent papers, e.g., [57] and [58], addressed UMP but few of them actually measure UMP. A method for measuring UMP by load cells was proposed in [59], but it had disadvantages: the amount of eccentricity did not remain constant as force is exerted, and a radial movement in eccentricity was noticed. A method for measurement of UMP was put forward in [60]. Piezoelectric transducers were used and the rotor and stator mounted separately. The stator was mounted on plate and rotor was mounted separately on pedestals. This method was quite effective.

A finite element analysis (FEA) was carried out for induction motor with open circuit and short circuit test and results recorded [61] and this gave details of the machine used here. A new test rig was setup to measure UMP of an induction motor under short circuit rotor and open circuit rotor [62] and this study is the basis for this thesis. The analytical results from [61] and [62] were analysed using condition monitoring methods [63], [65]. UMP varies with load and voltage in an induction motor and [66] studied this. The method of adding damper windings to machine has been proposed by different researchers [56], [67], and [68].

2.2. Research Development

The measurement and calculation of unbalanced magnetic pull in a wound rotor induction machine is still in need of further investigation; there is still little literature on the topic. There is extensive study of the cage induction machine in terms of UMP, including experimental measurement, but there is little research on the wound rotor induction machine. This

necessitates the measurement and development of methods for the reduction of UMP in order to maintain its performance since the maintenance cost of these machines is relatively high.

Harmonic winding analysis together with the air gap permeance harmonic method are use together here in order to put forward a method for calculating the UMP. Static eccentricity is used because this is likely to be the most common form or eccentricity and also it is more straightforward to put into the experimental rig.

Transducers are used to measure forces acting between the stator and rotor. They were integrated into the rotor mountings. Moving the stator horizontally, and also shimming vertically allowed the rotor to be centred and the UMP minimized. From here the rotor could be moved to put eccentricity into the machine in a controlled and measured way. The machine was a 4-pole machine so that additional 2-pole and 6-pole search windings were installed into the machine in spaces left by the removal of slot wedges. These allowed an eccentricity detection method to be investigated and they were also investigated to see if they could provide sufficient MMF to control the UMP. The former investigation proved successful with eccentricity easily detected with the pole-specific search coils. The latter investigation did prove unsuccessful.

Chapter 3: Analysis of Machine

Induction machines are extensively used as generators in the wind turbines. These machines, when in wound rotor form, operate at speeds both above and below the synchronous speed even when generating. Cage induction machines use a variable frequency inverter to vary the synchronous speed so that they can always operate super-synchronous and hence generate. The stator structures of both types of machine are similar, usually with distributed 3-phas windings. When a voltage source is connected to the windings, a magneto motive force (MMF) wave is produced in the air gap when the current flows. The rotor structures are also similar to each other but the short circuited squirrel cage winding is replaced by a three phase insulated distributed winding in wound rotor machine and this winding is accessed via slip rings. The rotor windings are wye connected and attached to three slip rings. These slip rings are further connected to the graphite brushes to provide access to rotor windings as shown in Fig. 3.1.

In this section some fundamental theory of an induction machine will be put forward in terms of defining the slip and developing expressions for the torque from the equivalent circuit. After this more specific analysis is developed in relation to machine operation with an eccentric rotor.

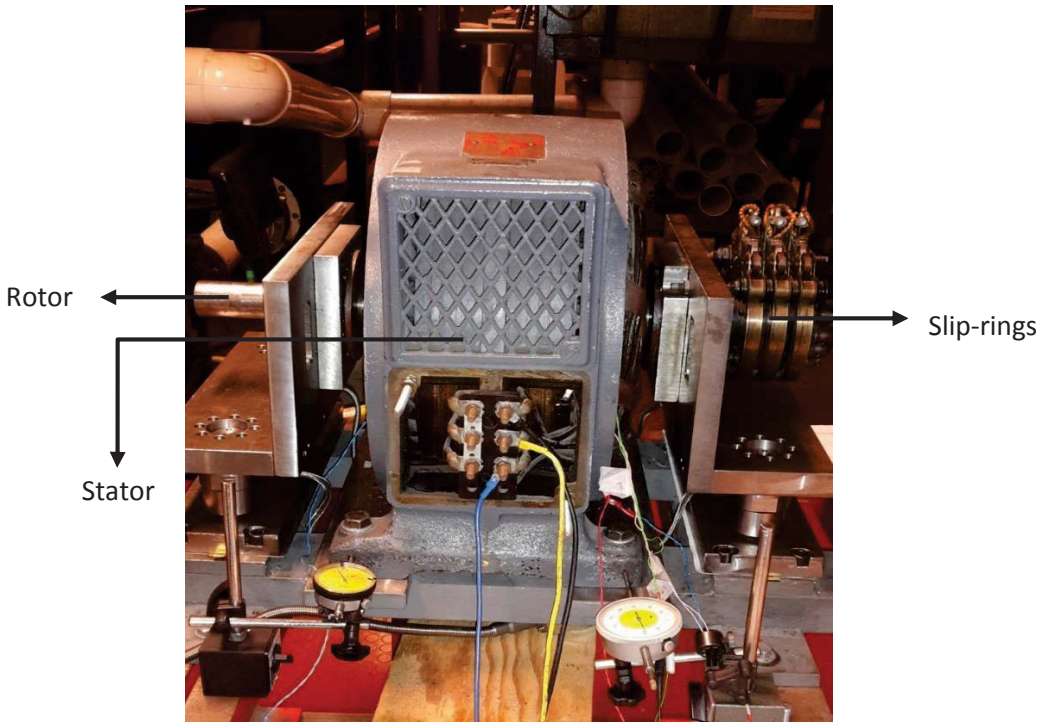

Figure 3.1: Rig including slip rings and graphite brushes.

3.1. Machine Slip

Induction machine operate at a speed slightly lower than synchronous speed n_s when operating as a motor and just above the synchronous speed when generating. When operating as a DFIG, where voltages are applied to the wound rotor circuit, the machine can operate well below and above the synchronous speed. It is important to calculate the slip of the induction motor which is defined by

$$s = \frac{n_s - n_r}{n_s} \text{ p.u.} \tag{3.1}$$

where n_s is the synchronous speed and n_r is the mechanical speed of the rotor.

The synchronous speed of an induction machine is dependent on the machine pole number and the frequency of the supply to the machine. It can be expressed as:

$$n_s = \frac{60\ f_e}{p} \text{ rpm} \tag{3.2}$$

where f_e is the electrical frequency of the supply and p is the machine pole-pairs. For determining frequency of the fundamental rotor frequency f_r (the slip frequency) the slip and supply frequency are used:

$$f_r = sf_e \text{ Hz} \tag{3.3}$$

This relationship shows that the rotor frequency as a product of slip and electrical frequency and that the rotor frequency varies with slip with constant supply frequency.

3.2. Torque

The DFIG machine is a wound rotor induction machine where both the stator and rotor are supplied separately. The stator is grid connected and the rotor is connected to an inverter to generate voltage sets of different slip frequencies. A rotor magnetic field is established due to rotor currents and it reacts with the stator magnetic field which results in torque. The torque magnitude is determined by angular displacement and by the magnitude of the product of both the fields. The maximum torque occurs when the vectors are in quadrature to each other as shown in Fig. 3.2. When a balanced 3-phase source in fed to the stator winding, stator flux is generated with a constant magnitude and it rotates with a synchronous speed. In this state, with

a rotor open-circuit, there is a no current flow and there is no production of rotor field $\bar{\Psi}_r$ so no torque is produced. When the rotor is short circuited so that the stator flux induces rotor EMFs, or the rotor is connected to a separate slip-frequency supply, current flows in the rotor and produces rotor magnetic flux $\bar{\Psi}_r$. This flux rotates at the same mechanical speed of the stator flux $\bar{\Psi}_s$. The torque produced by interaction of two fields is

$$T \propto j\bar{\Psi}_s \cdot \bar{\Psi}_r = |\Psi_s||\Psi_r|\sin\theta_t \quad \text{Nm} \tag{3.4}$$

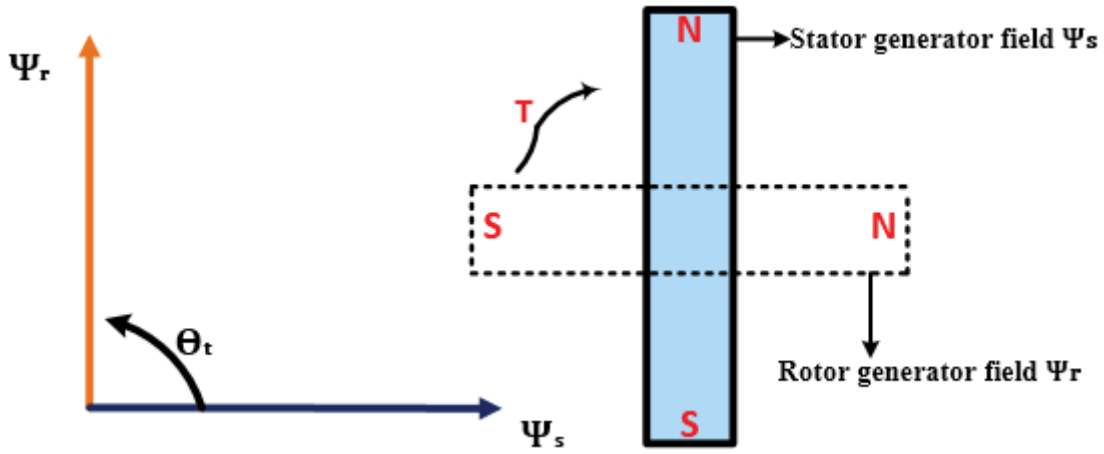

Figure 3.2: Magnetic pole system generated by currents in the stator and rotor windings.

These flux waves rotate at the same synchronous speed with respect to stationary state. The turning of rotor may be asynchronous but the rotational speed of rotor flux is same as the rotational speed of stator flux. The mechanical torque is related to the power absorbed by resistance component $R_r(1-s)$ in the per-phase equivalent circuit (Fig. 3.3) and also, if the machine is a wound rotor machine in a DFIG arrangement, the difference between the actual slip-frequency power from the rotor inverter and the power apparently flowing into the rotor in the equivalent circuit from V_r. When the rotor is shorted, the mechanical power is calculated from

$$P_{mech} = 3\,|i_r|^2\left(\frac{1-s}{s}\right)R_r \quad \text{W} \tag{3.5}$$

where

R_s = stator winding resistance

L_s = stator leakage reactance

R_r = rotor winding resistance

L_r = rotor leakage reactance

L_m = magnetizing reactance

sk is the effective stator : rotor turns ratio

s is the slip of the motor.

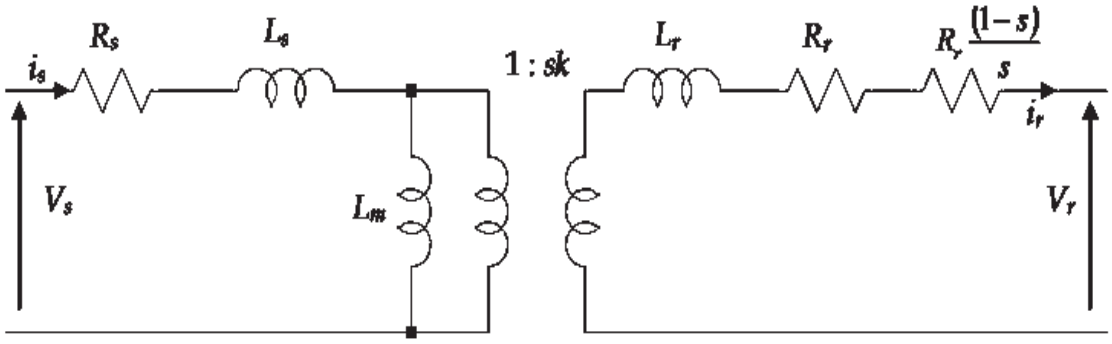

Figure 3.3: Equivalent circuit

Fig. 3.4 shows a simplified equivalent circuit with winding resistances and leakage inductances neglects and the machine phasor diagram which illustrates that for optimal conditions for torque production, the magnetizing flux is normal to the phasor of rotor current and flux.

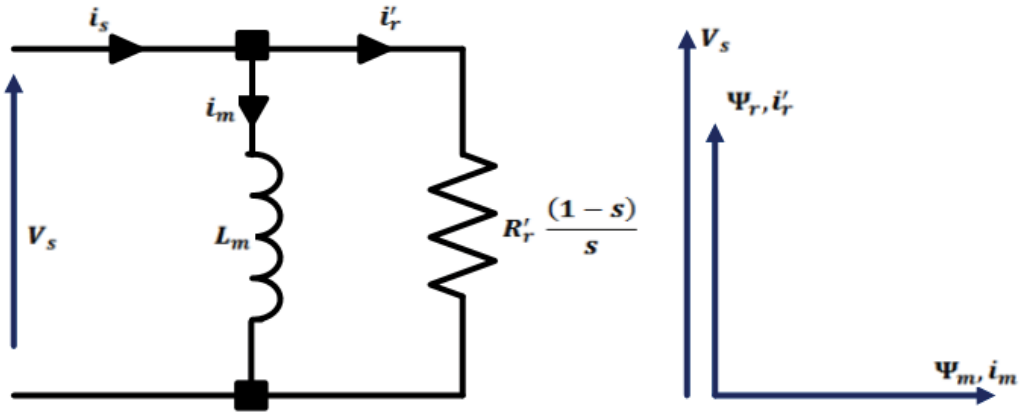

Figure 3.4: Simplified Equivalent circuit

Using the simplified circuit in Fig. 3.4 the mechanical torque is expressed using

$$P = T\omega \tag{3.6}$$

$$T = P/\omega \tag{3.7}$$

$$T_{mech} = 3\,|\,i_r^{/}\,|^2\left(\frac{1-s}{s}\right)\frac{R_r^{/}}{\omega_m} \qquad \text{Nm} \tag{3.8}$$

where

T = motor torque

ω_m is the mechanical rotational velocity.

The mechanical rotational velocity is obtained from

$$\frac{\omega_m}{\omega_s} = \frac{1-s}{p} \tag{3.9}$$

After simplification:

$$\omega_m = \frac{(1-s)\,\omega_s}{p} \quad \text{rpm} \tag{3.10}$$

Substituting (3.10) in (3.8), we get:

$$T_{mech} = 3\,|\,i_r^{/}\,|^2\left(\frac{1-s}{s}\right)\frac{R_r^{/}}{(1-s)\,\omega_s/p} = 3\,|\,i_r^{/}\,|^2\,\frac{R_r^{/}}{\omega_s/p} = \frac{3p\,|\,i_r^{/}\,|^2\,R_r^{/}}{s\omega_s} \quad \text{Nm} \tag{3.11}$$

The stator generated flux is expressed as

$$\Psi_m = L_m i_m \qquad \text{Wb} \tag{3.12}$$

$$\Psi_m = L_m i_m = v_s/\omega_s = \frac{\left|i_r^{/}\right| R_r^{/}}{s\omega_s} \qquad \text{Wb} \tag{3.13}$$

Replacing $\frac{\left|i_r^{/}\right| R_r^{/}}{s\omega_s}$ in Eq. 3.11 gives

$$T_{mech} = 3p\Psi_m\left|i_r^{/}\right| \quad \text{Nm} \tag{3.14}$$

The above expression shows that the magnitude of rotor current $i_r^{/}$ and the generated stator flux Ψ_m control the torque T_{mech} if both vectors are maintained as in Fig. 3.4.

To obtain the desired torque in a DFIG the rotor currents are regulated in such a way that its magnitude and the magnitude of stator flux act normal to each other but one is rotated by 180 deg electrical so that the torque is now negative. The generation of stator flux magnitude and the physical position of the rotor control the torque in a DFIG.

3.3. Air Gap Length

In this section a thorough derivation of the expression for the air gap length is given when the rotor is eccentric. This is then inverted to obtain an expression for the air gap permeance. This is done for completeness of the analysis.

There is an air gap between stator and rotor which plays an important role on the performance of the machine. The power factor, magnetising current, noise, cooling and overload capacity are greatly affected by air gap length. Induction machine are designed taking into consideration the air gap length for the performance of motor. In order to analyse the air gap length in a machine consider the stator and rotor as cylinders as shown in Fig. 3.5.

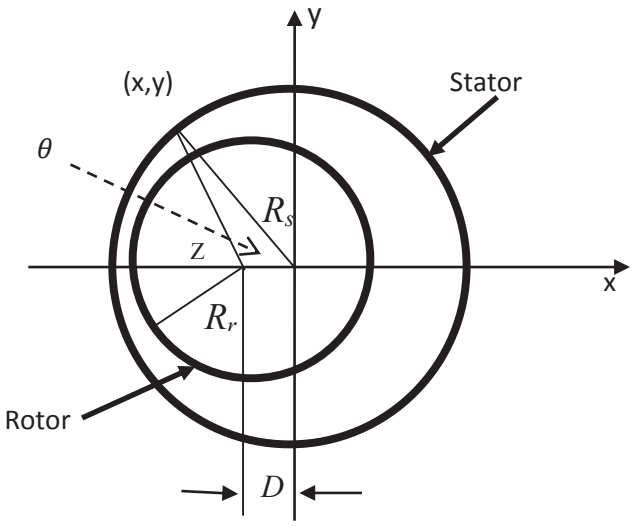

Figure 3.5: rotor and stator positioning

The equation of a circle, which can be used to represent the rotor which is offset a distance D from the origin is

$$(D+x)^2 + y^2 = R_r^2 \tag{3.15}$$

D represents the difference between the stator and rotor centres. Expanding the Eq. 3.15

$$D^2 + 2Dx + x^2 + y^2 = R_r^{\,2} \tag{3.16}$$

Rearranging Eq. 3.16

$$x^2 + y^2 = R_r^{\,2} - 2Dx - D^2 \tag{3.17}$$

According to the Pythagoras theorem

$$x^2 + y^2 = z^2 \tag{3.18}$$

Substituting Eq. 3.18 in Eq. 3.17

$$z^2 = R_r^{\,2} - 2Dx - D^2 \tag{3.19}$$

Since $x = z\cos\theta$, using trigonometric equations and substituting in Eq. 3.19 we get

$$z^2 + 2Dz\cos\theta = R_r^{\,2} - D^2 \tag{3.20}$$

By rearranging we get:

$$z^2 + 2Dz\cos\theta + D^2\cos^2\theta = R_r^{\,2} - D^2 + D^2\cos^2\theta \tag{3.21}$$

$$(z + D\cos\theta)^2 = R_r^{\,2} - D^2\left(1 - \cos^2\theta\right) \tag{3.22}$$

$$(z + D\cos\theta)^2 = R_r^{\,2}\left[1 - \frac{D^2}{R_r^{\,2}}\left(1 - \cos^2\theta\right)\right] \tag{3.23}$$

$$(z + D\cos\theta) = R_r\sqrt{1 - \frac{D^2}{R_r^{\,2}}\left(1 - \cos^2\theta\right)} \tag{3.24}$$

$$(z + D\cos\theta) = R_r\sqrt{1 + \frac{D^2}{2R_r^{\,2}}\left(\cos 2\theta - 1\right)} \tag{3.25}$$

Since $$\left(1 - \cos^2\theta\right) = -\tfrac{1}{2}\left(\cos 2\theta - 1\right) \tag{3.26}$$

And $D << R_r$

$$\sqrt{1+\frac{D^2}{2R_r{}^2}\left(\cos 2\theta - 1\right)} \cong 1 \tag{3.27}$$

Therefore $z + D\cos\theta \cong R_r \; z + D\cos\theta \cong R_r$ (3.28)

$$z \cong R_r - D\cos\theta \tag{3.29}$$

The radial distance between rotor and stator g is assumed to be $g \cong z - R^2$ so that

$$g \cong R_r - D\cos\theta - R_s \tag{3.30}$$

$$g \cong R_r - R_s - D\cos\theta \tag{3.31}$$

Since $D = dg_{av}$ (3.32)

Then $g \cong g_{av}(1 - d\cos\theta)$ [m] (3.33)

where,

d = degree of rotor offset [p.u.]

D = difference between the stator and rotor centres [m]

g_{av} = effective air gap length when the rotor is concentric [m]

The above expression represents the air gap in between stator and rotor of the machine with static rotor eccentricity, as shown in Figure 3.3. The air gap length can be calculated using Eq. 3.33. This equation is expressed in axial (x) and circumferential (y) direction.

$$g(x,y) = g_{av}\left(1 - d(x)\cos\left(ky - \phi(x)\right)\right) \quad \text{[m]} \tag{3.34}$$

In exponential form using Euler's formula for a cosine

$$\cos\left(x\right) = \frac{e^{ix} + e^{-ix}}{2} \tag{3.35}$$

Eq.3.34 can be expressed as

$$g(x,y) = g_{av}\left(1 - \frac{d(x)}{2}\left(e^{j(ky-\phi(x))} - e^{-j(ky-\phi(x))}\right)\right) \tag{3.36}$$

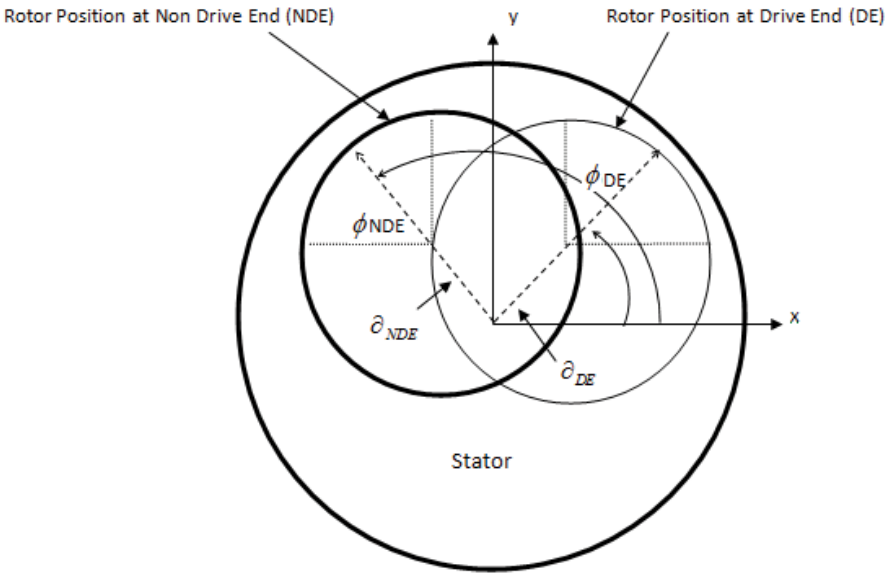

Figure 3.6: DE and NDE Eccentricity

Now as the motor have Drive End (DE) and Non Drive End (NDE) so,

$$g(x,y) = g_{av}\left[1 - 0.5\begin{pmatrix} d_{DE}(x)e^{j(ky-\phi_{DE})} + d_{NDE}(x)e^{j(ky-\phi_{NDE})} \\ + d_{DE}(x)e^{-j(ky-\phi_{DE})} + d_{NDE}(x)e^{-j(ky-\phi_{NDE})} \end{pmatrix}\right] \quad \text{[m]} \qquad (3.37)$$

This has to be inverted to obtain an expression for the inversion.

3.4. Permeance

The presence of rotor slots, stator slots, eccentricity of, and dissymmetric in, stator and rotor, and magnetic saturation results in pemeance wave of air gap. It is the inverse of air gap length.

$$P = 1/g \qquad (3.38)$$

Eq. 3.33 is used to determine air gap in between the stator and rotor of the motor, and substituting in 3.38, and assuming there is axial variation of the static eccentricity at each end

$$P = 1/g(x,y) = \frac{1}{g_{av}\left(1 - d(x,y)\cos\theta\right)} \qquad (3.39)$$

This becomes

$$P(x,y)=\frac{1}{g(x,y)}=\frac{1}{g_{av}\left[1-0.5\begin{pmatrix} d_{DE}(x)e^{j(ky-\phi_{DE})}+d_{NDE}(x)e^{j(ky-\phi_{NDE})} \\ +d_{DE}(x)e^{-j(ky-\phi_{DE})}+d_{NDE}(x)e^{-j(ky-\phi_{NDE})}\end{pmatrix}\right]} \tag{3.40}$$

So that

$$P(x,y)=\frac{1}{g(x,y)}=\frac{1}{g_{av}}\left[1-\begin{pmatrix} \partial_{DE}(x)e^{j(ky-\phi_{DE})}+\partial_{NDE}(x)e^{j(ky-\phi_{NDE})} \\ +\partial_{DE}(x)e^{-j(ky-\phi_{DE})}+\partial_{NDE}(x)e^{-j(ky-\phi_{NDE})}\end{pmatrix}\right] \quad [\text{m}] \tag{3.41}$$

where $\delta_{DE}(x)=\left(\frac{(L_{st}+2x)}{2d_{DE}L_{st}}\right)$ and $\delta_{NDE}(x)=\left(\frac{(L_{st}-2x)}{2d_{NDE}L_{st}}\right)$

This gives a general expression for the air gap eccentricity where it varies at each end. The axial $x = 0$ position is assumed to be at the axial centre of the machine.

3.5. Unbalanced Magnetic Pull

For determining the UMP, we need to calculate the current in stator and rotor windings. Using the coupling impedance method (shown later), the air gap flux density is divided into a harmonic series of waves rotating with different pole numbers in either direction. In the harmonic Fourier series of the surface current distributions, currents and positioning of the stator and rotor coils are required. This series is based on both time and space components. The complex Fourier analysis of the machine is used to obtain the conductor density distribution expression in terms of harmonic series. Complex Fourier analysis takes in account the magnitude and positioning of the conductors on the surface of stator and rotor.

In Fig. 3.7, a linearized machine surface is considered with x axial direction variation, y is the tangential direction variation and z is the radial direction variation. In this frame a coil with c turns is located. Fig. 3.7 shows the position of this single coil on the stator. The complex Fourier series can be expressed as

$$n(y)=\sum_{n=-\infty}^{\infty}\left(\bar{c}^{n}e^{-jnky}\right) \tag{3.42}$$

with

$$\bar{c}^{n}=\int_{y_1-b_s}^{y_1+b_s}\frac{c}{b_s}e^{jnky}.dy-\int_{y_2-b_s}^{y_2+b_s}\frac{c}{b_s}e^{jnky}.dy \tag{3.43}$$

where

c = number of coil turns

b_s = slot opening

y = variation in tangential direction

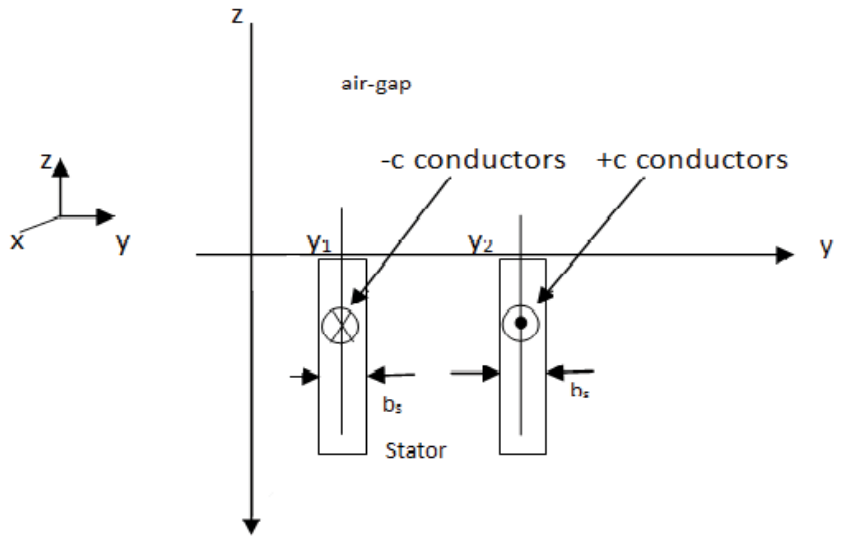

Figure 3.7: Position of coil on stator

Eq. 3.43 in exponential form is

$$\bar{c}^n = \int_0^{2\pi r} \frac{c}{b_s}\left(e^{jnky_1} - e^{jnky_2}\right).dy \tag{3.44}$$

$$\bar{c}^n = \frac{k_s^n c}{2\pi r}\left(e^{jnky} - e^{jnky_2}\right) \tag{3.45}$$

where $k_s^n = n^{th}$ harmonic stator slot opening factor which is defined as

$$k_s^n = \frac{\sin\left(nk\frac{b_s}{2}\right)}{nk\frac{b_s}{2}} \tag{3.46}$$

where $k = \frac{1}{r}$

r = average air gap radius,

b_s = stator slot opening.

For a set of series connected coils Eq. 3.34 can be expressed as

$$n_x(y) = \sum_{n=-\infty}^{\infty} \bar{N}_x^n e^{-jnky} \tag{3.47}$$

where n is the harmonic number = 1, 3, 5, etc. and

$$\bar{N}_x^n = \frac{1}{2\pi r} \sum_{\omega=1}^{N} k_s^n C_w e^{jnky_\omega} \tag{3.48}$$

C_w is the number of conductors in w^{th} slot and k_s^n is the slot opening factor which is close to unity and can initially be set to unity. The winding current is defined by

$$i_x(t) = \text{Re}\left[\bar{I}_x e^{j\omega t}\right] \tag{3.49}$$

The current density on surface is therefore

$$j_x(y,t) = \text{Re}\left[\sum_{n=-\infty}^{\infty} \left(\bar{N}_x^n \bar{I}_x e^{j(\omega t - nky)}\right)\right] \tag{3.50}$$

This is also known as the MMF wave on the surface. The stator MMF wave is

$$j_s(y,t) = \text{Re}\left[\sum_{n=-\infty}^{\infty} \left(\bar{N}_s^n \bar{I}_s e^{j(\omega t - nky)}\right)\right] \tag{3.51}$$

The rotor conductor distribution is also obtained similar manner to stator

$$j_r(y,t) = \text{Re}\left[\sum_{n=-\infty}^{\infty} \left(\bar{N}_r^n \bar{I}_r e^{j(\omega t - nky)}\right)\right] \tag{3.52}$$

The rotor with conductors can be represented similar to stator as shown in Figure 3.7. The conductor distribution will be

$$n_r(y) = \sum_{n=-\infty}^{\infty} \left(\bar{N}_r e^{j(-nky)}\right) \tag{3.53}$$

where $$\bar{N}_r = \frac{k_r^n e^{jnky}}{2\pi r} \tag{3.54}$$

and the rotor slot opening factor is

$$k_r^n = \frac{\sin(nk)}{nk} \tag{3.55}$$

where l = number of loop.

y = tangential direction variation.

k = average gap radius.

The flux density due to current distribution can be calculated using Ampere's law as

$$b(y,t) = \int \frac{j(y,t)}{g(y)}.dy \tag{3.56}$$

$$b(y,t) = \mathrm{Re} \sum_{n=-\infty}^{\infty} \bar{B}_s^{np_m} e^{j(\omega t - np_m ky)} \tag{3.57}$$

The electric field can be calculated from

$$e(y,t) = \int \frac{d\,b(y,t)}{dt}.dy \tag{3.58}$$

This is also known as the air gap EMF wave. When the machine is in the state of static eccentricity in the direction of displacement the normal stresses in the air gap can be expressed by Maxwell stress.

$$\sigma_n = \frac{b_n^2(y,t) - b_t^n(y,t)}{2\mu_0} \tag{3.59}$$

where n indicates normal component and t indicates tangential component. The normal component of the flux density can be obtained from

$$b_n(y,t) = \frac{\mu_0}{\mathrm{g}(y)}\left(\int j(y,t).dy + C\right) \tag{3.60}$$

where μ_0 is the permeance of free space. At no load the tangential component $b_t(y,t)$ is relatively small compared to $b_n(y,t)$ and is neglected so that

$$\sigma_n = \frac{b_n^2(y,t)}{2\mu_o} \tag{3.61}$$

Since the air gap flux density $b_n(y,t)$ is a function of MMF and total permeance P and is a function of rotor position with respect to time. Then air gap flux $b_n(y,t)$ is

$$b_n(y,t) = \mu_o P \int j_x(y,t)\,dy = \frac{\mu_o}{g_{av}(1-\partial\cos\theta)} \int j_x(y,t)\,dy \tag{3.62}$$

So Maxwell stress becomes

$$\sigma = \frac{\left(\frac{\mu_0}{g_{av}(1-\partial\cos\theta)} \int j_x(y,t)\,dy \right)^2}{2\mu_O} \tag{3.63}$$

Solving Eq. 3.63 further we get

$$\sigma = \frac{\mu_o^2 \left(\int j_x(y,t)\,dy \right)^2}{g_{av}(1-\partial\cos\theta)^2 \times 2\mu_o} \tag{3.64}$$

$$\sigma = \frac{\mu_o \left(\mathrm{Re}\left[\sum_{n=-\infty}^{\infty} \left(\bar{N}_x^n \bar{I}_x e^{j(\omega t - nky)} \right) \right] \right)^2}{2(nkg_{av})^2 (1-\partial\cos\theta)^2} \tag{3.65}$$

Using the Maxwell stress, the force components in the x and y directions can be calculated from

$$F_x = \int_0^{2\pi} \sigma rL \cos\theta\, d\theta \tag{3.66}$$

$$F_x = \int_0^{2\pi} \frac{\mu_o \left(\mathrm{Re}\left[\sum_{n=-\infty}^{\infty} \left(\bar{N}_x^n \bar{I}_x e^{j(\omega t - nky)} \right) \right] \right)^2}{2(nkg_{av})^2 (1-\partial\cos\theta)^2} rL \cos\theta\, d\theta \tag{3.67}$$

and

$$F_y = \int_0^{2\pi} \sigma rL \sin\theta\, d\theta \tag{3.68}$$

$$F_y = \int_0^{2\pi} \frac{\mu_o \left(\mathrm{Re}\left[\sum_{n=-\infty}^{\infty} \left(\bar{N}_x^n \bar{I}_x e^{j(\omega t - nky)} \right) \right] \right)^2}{2(nkg_{av})^2 (1-\partial\cos\theta)^2} rL \sin\theta\, d\theta \tag{3.69}$$

where r = Mean air gap radius.

L = Axial length of the stator.

The equations help in the understanding and calculation of the UMP in the machine. It can be seen in the denominator that there is a $(1 - \delta \cos \theta)^2$ term inside the integral. Even when worked through it can be seen that the UMP is approximately proportional the degree of eccentricity.

3.6. Addition of 2 pole and 6 pole Windings

The Machine is modified with the addition of 2 pole and 6 pole windings located in space at the top of the slots. This space was obtained by the remove for slot wedges. The machine is old and the windings was ridged so that these could be removed. This was done to assess a method for measuring the eccentricity and also to the UMP in the machine taking axial variation in the eccentricity into account. These two pole and six pole windings are introduced as shown in Fig. 3.9. There was one 6-pole winding and also two 2-pole windings in quadrature. The winding diagram of these 2-pole and 6 pole search windings are shown in Appendices C and D respectively. The machine specification is given in Appendix A and the main windings given in Appendix B.

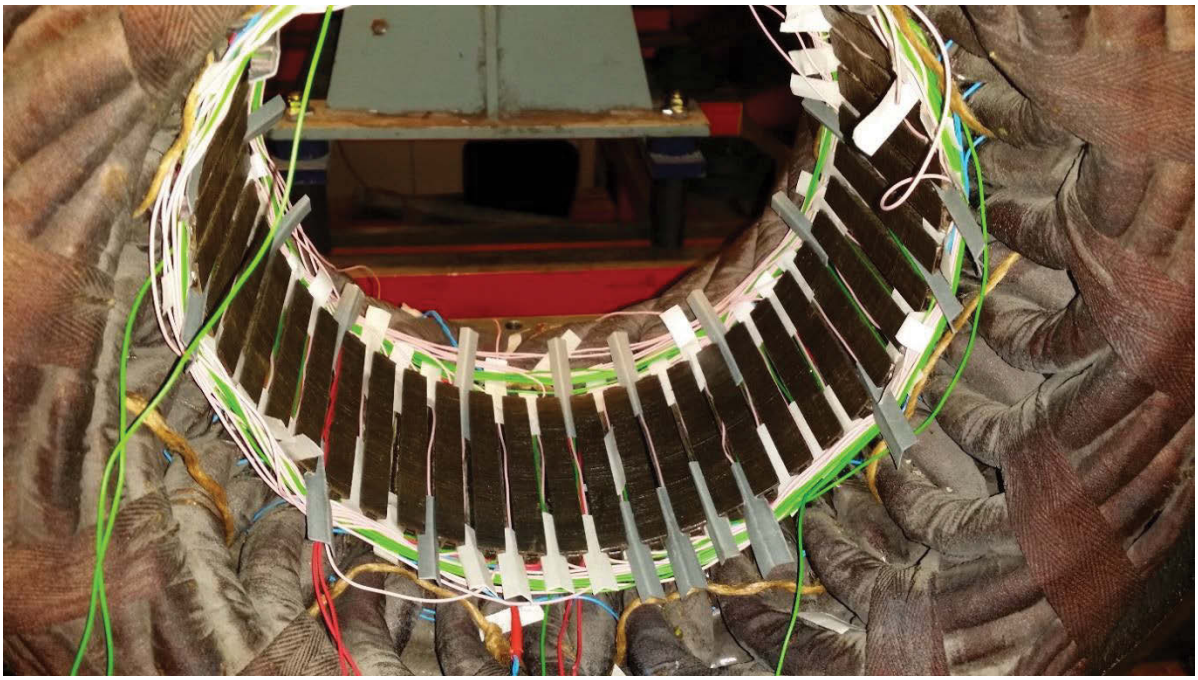

Figure 3.9: 2-pole and 6-pole search winding

In a machine, a series of the flux waves contribute to the production of UMP in the motor. For the generation of additional air gap flux waves, permeance modulation due to eccentricity is utilized to produce a rotating electric field in the air gap with the correct pole number to induce voltages in the pole-specific search windings. In this instance, for the 4-pole winding, voltages are induced in the 2-pole and 6-pole search windings. If the windings with more turns and MMF capacity were used for the search coils then they can be short circuited and the induced voltage generate current. This current will set up air gap flux waves too and these will oppose the voltage-inducing flux waves, i.e., they will damp the UMP. This is similar the effect of using parallel windings.

For determining additional air gap flux waves in motor the MMF equation (Eq. 3.53) is used.

$$j_s\left(y,t\right)=\mathrm{Re}\sum_{n=-\infty}^{\infty}\left[\bar{N}_s^n\bar{I}_s e^{j(\omega t-nky)}\right] \tag{3.70}$$

where $\bar{N}_s^n\bar{I}_s=\bar{J}_s^n$

Substituting in Eq. 3.70

$$j_s\left(y,t\right)=\mathrm{Re}\sum_{n=-\infty}^{\infty}\bar{J}_s^n e^{j(\omega t-nky)} \tag{3.71}$$

Using the identity $a=\exp\left(j2\pi/3\right)$ for a balanced 3 phase current, then

$$\bar{J}_s^n=\bar{N}_s^n\left(1+a^{n-1}+a^{1-n}\right)\bar{I}_s \tag{3.72}$$

$$\bar{J}_s^n=\bar{N}_s^n\left(1+a^{n-1}+a^{1-n}\right)\bar{I}_s=3\bar{N}_s^n\bar{I}_s\Big|_{n=1,-5,7} \tag{3.73}$$

For a machine pole-pair number p_m, Eq. 3.71 is modified to

$$j_s\left(y,t\right)=\mathrm{Re}\sum_{n=-\infty}^{\infty}\bar{J}_s^n e^{j(\omega t-np_mky)} \tag{3.74}$$

Modifying Eq. 3.48, stator winding coefficient of single phase winding is obtained

$$\bar{N}_s^n=\frac{k}{2\pi}\sum_{w=1}^{N_w}k_s C_w e^{j_n p_m k y_w} \tag{3.75}$$

As we know $k = 1/r$ substituting in Eq. 3.75

$$\bar{N}_s^n = \frac{1}{2\pi r}\sum_{w=1}^{N_w} k_s C_w e^{j_n p_m k y_w} \tag{3.76}$$

Where p_m = pole pair number of the machine

N_w = Number of slot where the winding is located

C_w = Number of conductors in w^{th} slot

Using Eq. 3.46, the slot opening factor k_s can expressed as

$$k_s = \frac{2\sin\left(0.5n\, p_m k b_s\right)}{n\, p_m k b_s} \tag{3.77}$$

The flux density in the stator due to current distribution is calculated using Ampere's law as in Eq. 3.56. Eq. 3.73 is substituted in Eq. 3.56 and modified to get the mathematical expression.

$$b_s\left(x,y,t\right) = \frac{\mu_0}{g_s\left(x,y\right)}\int j_s\left(y,t\right)dy \tag{3.78}$$

Ampere's circuital law can be applied using the equation

$$b_s(x,y,t) = \mu_o \Lambda_s(x,y)\left[\int j_s(y,t)dy + C\right] \tag{3.79}$$

This leads to

$$b_s(x,y,t) = \mathrm{Re}\sum_{n=-\infty}^{\infty}\left[\bar{B}_s^{np_m} e^{j(\omega t - np_m k y)} + \bar{B}_s^{np_m-1}(x)e^{j(\omega t - k(np_m-1)y)} + \bar{B}_s^{np_m+1}(x)e^{j(\omega t - k(np_m+1)y)}\right] \tag{3.80}$$

Eq. 3.80 expresses the air gap flux distribution and shows the additional flux waves where

$\bar{B}_s^{np_m} = \dfrac{j\mu_0 \bar{J}_s^n}{knp_m g_{av}}$ and $\bar{B}_s^{np_m\pm1}(x) = \dfrac{j\mu_0 \bar{J}_s^n}{knp_m g_{av}}\bar{\delta}(x)$ represent flux density magnitudes.

In the similar manner Eq. 3.57, this can be used to calculate the EMFs in the additional windings. Substituting Eq. 3.77 in Eq. 3.58 we get the stator EMFs:

$$e_s(x,y,t) = \int \frac{db_s(x,y,t)}{dt} dy \tag{3.81}$$

$$e_s(x,y,t) = \bar{E}_s^{p_m \pm 1}(x) e^{j(\omega t - k(p_m \pm 1)y)} \tag{3.82}$$

where $$\bar{E}_s^{p_m \pm 1}(x) = \frac{-\bar{B}_s^{np_m \pm 1}(x)}{k(p_m \pm 1)} = \frac{-j\mu_0 \omega \bar{J}_s^n}{k^2 p_m (p_m \pm 1) g_{av}} \bar{\delta}(x) \tag{3.83}$$

For obtaining expressions for induced EMFs in these windings, the following expressions are used which are modified according to each pole pair number which has two windings in α and β axes quadrature.

$$\xi_{(h+1)}(\alpha,\beta,t) = \mathrm{Re} \int_{-ls/2}^{ls/2} \int_{0}^{2\pi r} -e^{p_{m+1}}(x,y,t) n_{(h+1)(\alpha,\beta)}^{p_{m+1}}(y) dy dx \tag{3.84}$$

$$\xi_{(h-1)}(\alpha,\beta,t) = \mathrm{Re} \int_{-ls/2}^{ls/2} \int_{0}^{2\pi r} -e^{p_{m-1}}(x,y,t) n_{(h-1)(\alpha,\beta)}^{p_{m-1}}(y) dy dx \tag{3.85}$$

where $$n_{(h+1)\alpha}^{p_{m+1}}(y) = \bar{N}_{(h+1)\alpha}^{p_{m+1}} e^{j(p+1)ky}, \tag{3.86}$$

$$n_{(h+1)\beta}^{p_{m+1}}(y) = j\bar{N}_{(h+1)\beta}^{p_{m+1}} e^{j(p+1)ky}, \tag{3.87}$$

$$n_{(h-1)\alpha}^{p_{m-1}}(y) = \bar{N}_{(h-1)\alpha}^{p_{m-1}} e^{j(p-1)ky}, \tag{3.88}$$

and $$n_{(h-1)\beta}^{p_{m-1}}(y) = j\bar{N}_{(h-1)\beta}^{p_{m-1}} e^{j(p-1)ky} \tag{3.89}$$

where $\bar{N}_{(h\pm1)}^{p_m \pm 1}$ is defined using Eq. 3.76

$$\bar{N}_{(h+1)}^{p_{m+1}} = \frac{1}{2\pi r} \sum_{\omega=1}^{N_w} k_s C_{w(h+1)} e^{jn(p_m+1)ky_w} \tag{3.90}$$

And $$\bar{N}_{(h-1)}^{p_{m-1}} = \frac{1}{2\pi r} \sum_{\omega=1}^{N_\omega} k_s C_{\omega(h-1)} e^{jn(p_m-1)ky_\omega} \tag{3.91}$$

where h = search coil numbers

Ignoring the winding harmonics in the motor, so with n =1, air gap flux is represented as follows using Eq. 3.80

$$b_s(x,y,t) \approx \left(\overline{B}_s^{p_m} e^{j(\omega t - p_m k y)} + \overline{B}_s^{p_m-1}(x) e^{j(\omega_1 t - k(p_m-1)y)} + \overline{B}_s^{p_m+1}(x) e^{j(\omega_2 t - k(p_m+1)y)} \right) \quad (3.92)$$

For the DE and NDE of the machine as shown in Fig. 2.5, $B_s^{(np_m \pm 1)}(x)$ is applied to both DE and NDE in order to calculate the UMP from Eq.3.60 so that

$$\sigma_s = \frac{b_s(x,y,t)^2}{2\mu_0}$$

$$\sigma_s = \frac{\left(\overline{B}_s^{p_m} e^{j(\omega t - p_m k y)} + \overline{B}_s^{p_m-1}(x) e^{j(\omega_1 t - k(p_m-1)y)} + \overline{B}_s^{p_m+1}(x) e^{j(\omega_2 t - k(p_m+1)y)} \right)^2}{2\mu_0} \quad (3.93)$$

And Force for *x* and *y* components is calculated by

$$F_x = \int_0^{2\pi} \sigma_s \, rL \cos\theta \, d\theta$$

$$F_x = \int_0^{2\pi} \frac{\left(\overline{B}_s^{p_m} e^{j(\omega t - p_m k y)} + \overline{B}_s^{p_m-1}(x) e^{j(\omega_1 t - k(p_m-1)y)} + \overline{B}_s^{p_m+1}(x) e^{j(\omega_2 t - k(p_m+1)y)} \right)^2}{2\mu_0} rL \cos\theta \, d\theta \quad (3.94)$$

$$F_y = \int_0^{2\pi} \sigma_s \, rL \sin\theta d\theta$$

$$F_y = \int_0^{2\pi} \frac{\left(\overline{B}_s^{p_m} e^{j(\omega t - p_m k y)} + \overline{B}_s^{p_m-1}(x) e^{j(\omega_1 t - k(p_m-1)y)} + \overline{B}_s^{p_m+1}(x) e^{j(\omega_2 t - k(p_m+1)y)} \right)^2}{2\mu_0} rL \sin\theta \, d\theta \quad (3.95)$$

3.7. UMP Attenuation by Additional Windings

The main purpose of this test is to measure the attenuation on UMP caused by the MMFs in the search windings which can be utilized as damper windings if they have sufficient turns and MMF capacity. They are short circuited or even additional voltage can be injected. The use of these damper windings has been used elsewhere. In terms of condition monitoring of the open circuit search coils winding (voltage), or short circuit damper winding (current), it does appear to be a straight forward method of detecting machine functional faults and the maintenance

costs are reduced due to at early stages detection. This helps in minimizing the chances of motor failure in plants.

In the past extensive work was carried out for the detection of faults using condition monitoring. Hwang *et al*. [69] mentioned flux monitoring as an accurate and reliable techniques for acquiring information on the electrical machine condition. A set of equations is put forward in [70], [71] that inspect the relationships between the air gap flux, stator current, air gap eccentricity and vibration signal. Search coils were included at the rear of the machine to determine the eccentricity and rotor bar faults on the basis of measurement of leakage flux in [72]. The main purpose of using the leakage flux measurement is its ease of implementation. In [73], Verma *et al*. presented work and stated that the change of the air gap flux density is a function of static eccentricity. The utilization of special flux sensors for condition monitoring of electrical drives was presented by Frosini *et al*. [74]. Placement of search coils under the wedges of stator winding of a motor is done in order to measure the actual magnetic flux was used in [75]. The same methodology of placing search coils under the wedges of stator windings in a machine is used in our experiment to detect the winding voltages. For this purpose the development of an independence matrix is required.

$$V = \overline{Z} i \tag{3.96}$$

Where V is the induced voltage, Z as an impedance and I is the induced current in the windings. In order to simplify the analysis then the machine is assumed to have an open circuit rotor and running light. Eq (3.96) can be written in the form of matrix as:

$$\begin{bmatrix} v_{ph} \\ v^{\alpha}_{pm-1} \\ v^{\beta}_{pm-1} \\ v^{\alpha}_{pm+1} \\ v^{\beta}_{pm+1} \end{bmatrix} = \left[\overline{Z}\right] \begin{bmatrix} i_{ph} \\ 0 \\ 0 \\ 0 \\ 0 \end{bmatrix} \tag{3.97}$$

$$\begin{bmatrix} v_{ph} \\ v_{pm-1}^{\alpha} \\ v_{pm-1}^{\beta} \\ v_{pm+1}^{\alpha} \\ v_{pm+1}^{\beta} \end{bmatrix} = \begin{bmatrix} \bar{Z}_{ph,ph} & 0 & 0 & 0 & 0 \\ \bar{Z}_{pm-1,ph}^{\alpha} & 0 & 0 & 0 & 0 \\ \bar{Z}_{pm-1,ph}^{\beta} & 0 & 0 & 0 & 0 \\ \bar{Z}_{pm+1,ph}^{\alpha} & 0 & 0 & 0 & 0 \\ \bar{Z}_{pm+1,ph}^{\beta} & 0 & 0 & 0 & 0 \end{bmatrix} \begin{bmatrix} i_{ph} \\ 0 \\ 0 \\ 0 \\ 0 \end{bmatrix} \tag{3.98}$$

where $$\bar{Z}_{ph,ph} = R_{ph} + jX_{leakage} + jX_{mag} \tag{3.99}$$

and jX_{mag} can be abstracted from the following simplification using the expression for EMF:

$$\xi_{(h)}(t) = \mathrm{Re} \int_{-ls/2}^{ls/2} \int_{0}^{2\pi r} -e_s^{p_m}(x,y,t)\, n_s^{p_m}(y)\, dy dx \tag{3.100}$$

where $$e_s^{p_m}(x,y,t) = \bar{E}_s^{P_m}(x) e^{j(\omega t - k(p_m)y)} \tag{3.101}$$

$$\bar{E}_s^{p_m}(x) = \frac{-\bar{B}_s^{np_m}(x)}{kp_m} = \frac{-j\mu_0 \omega \bar{J}_s^n}{k^2 p_m^2 g_{av}}, \tag{3.102}$$

$$n_s^{p_m}(y) = \left(\bar{N}_s^{p_m}\right) e^{-jp_m k y} \tag{3.103}$$

and $$\bar{J}_s^n = 3\bar{N}_s^n \bar{I}_s \Big|_{n=1,-5,7} \tag{3.104}$$

It is relatively straightforward to extend the analysis to include the rotor current, and this will be the focus of future work. Substitute Eq. (3.104) in Eq. (3.102), Eq. (3.102) in Eq. (3.101), and Eq. (3.101) and Eq. (3.103) into Eq. (3.104). After simplification we obtain:

$$\xi_h(t) = \mathrm{Re}\left[j X \bar{I}_s e^{j\omega t} \right] \tag{3.105}$$

And the value of

$$X = \frac{3\pi\mu_0 \omega L_{st} \bar{N}_{st}^1}{k^3 p_m^2 g_{av}} \left(\bar{N}_{st}^1\right)^* \tag{3.106}$$

which is X_{mag} and is known as the magnetizing reactance. The other two factors: tooth MMF and core back MMF in Eq. (3.99), can be neglected depending on the design and manufacture of the machine. In a similar manner the expressions for other impedances are obtained from

$$\bar{Z}^{\alpha}_{pm-1,ph} = j\frac{3\pi\mu_0\omega L_s \bar{N}_s^1}{k^3 p_m\left(p_m-1\right)g_{av}}\bar{\delta}(\text{mean})\left(\bar{N}^{p_m-1}_{(h-1)}\right)^* \tag{3.107}$$

$$\bar{Z}^{\beta}_{pm-1,ph} = j\frac{3\pi\mu_0\omega L_s \bar{N}_s^1}{k^3 p_m\left(p_m-1\right)g_{av}}\bar{\delta}(\text{mean})\left(j\bar{N}^{p_m-1}_{(h-1)}\right)^* \tag{3.108}$$

$$\bar{Z}^{\alpha}_{pm+1,ph} = j\frac{3\pi\mu_0\omega L_s \bar{N}_s^1}{k^3 p_m\left(p_m+1\right)g_{av}}\bar{\delta}(\text{mean})\left(\bar{N}^{p_m-1}_{(h+1)}\right)^* \tag{3.109}$$

$$\bar{Z}^{\beta}_{pm+1,ph} = j\frac{3\pi\mu_0\omega L_s \bar{N}_s^1}{k^3 p_m\left(p_m+1\right)g_{av}}\bar{\delta}(\text{mean})\left(j\bar{N}^{p_m-1}_{(h+1)}\right)^* \tag{3.110}$$

For control of UMP additional winding currents are introduced into Eq. (3.98), then

$$\begin{bmatrix} v_{ph} \\ 0 \\ 0 \\ 0 \\ 0 \end{bmatrix} = \begin{bmatrix} \bar{Z}_{ph,ph} & \bar{Z}^{\alpha}_{ph,pm-1} & \bar{Z}^{\beta}_{ph,pm-1} & \bar{Z}^{\alpha}_{ph,pm+1} & \bar{Z}^{\beta}_{ph,pm+1} \\ \bar{Z}^{\alpha}_{pm-1,ph} & \bar{Z}^{\alpha}_{pm-1,ph} & 0 & 0 & 0 \\ \bar{Z}^{\beta}_{pm-1,ph} & 0 & \bar{Z}^{\beta}_{pm-1,ph} & 0 & 0 \\ \bar{Z}^{\alpha}_{pm+1,ph} & 0 & 0 & \bar{Z}^{\alpha}_{pm+1,ph} & 0 \\ \bar{Z}^{\beta}_{pm+1,ph} & 0 & 0 & 0 & \bar{Z}^{\beta}_{pm+1,ph} \end{bmatrix} \begin{bmatrix} i_{ph} \\ i^{\alpha}_{pm-1} \\ i^{\beta}_{pm-1} \\ i^{\alpha}_{pm+1} \\ i^{\beta}_{pm+1} \end{bmatrix} \tag{3.111}$$

If the windings are shortened then

$$\bar{Z}^{\alpha}_{ph,pm-1} = j\frac{\pi\mu_0\omega L_s \bar{N}_s^{-1}}{k^3 p_m\left(p_m-1\right)g_{av}}\bar{\delta}(\text{mean})\left(\bar{N}^{p_m-1}_{(h-1)}\right) \tag{3.112}$$

$$\bar{Z}^{\beta}_{ph,pm-1} = j\frac{\pi\mu_0\omega L_s \bar{N}_s^{-1}}{k^3 p_m\left(p_m-1\right)g_{av}}\bar{\delta}(\text{mean})\left(j\bar{N}^{p_m-1}_{(h-1)}\right) \tag{3.113}$$

$$\bar{Z}^{\alpha}_{ph,pm+1} = j\frac{\pi\mu_0\omega L_s \bar{N}_s^{-1}}{k^3 p_m\left(p_m+1\right)g_{av}}\bar{\delta}(\text{mean})\left(\bar{N}^{p_m+1}_{(h+1)}\right) \tag{3.114}$$

$$\bar{Z}^{\beta}_{ph,pm+1} = j\frac{\pi\mu_0\omega L_s \bar{N}_s^{-1}}{k^3 p_m\left(p_m+1\right)g_{av}}\bar{\delta}(\text{mean})\left(j\bar{N}^{p_m+1}_{(h+1)}\right) \tag{3.115}$$

UMP can also be obtained in the similar manners as expressed

$$\begin{bmatrix} F_\alpha \\ F_\beta \end{bmatrix} = \begin{bmatrix} F_{\alpha,ph} & F^{\alpha}_{\alpha,pm-1} & F^{\beta}_{\alpha,pm-1} & F^{\alpha}_{\alpha,pm+1} & F^{\beta}_{\alpha,pm+1} \\ F_{\beta,ph} & F^{\alpha}_{\beta,pm-1} & F^{\beta}_{\beta,pm-1} & F^{\alpha}_{\beta,pm+1} & F^{\beta}_{\beta,pm+1} \end{bmatrix} \begin{bmatrix} i_{ph} \\ i^{\alpha}_{pm-1} \\ i^{\beta}_{pm-1} \\ i^{\alpha}_{pm+1} \\ i^{\beta}_{pm+1} \end{bmatrix} \tag{3.116}$$

This outlines the method that can be used to damp and control the UMP through axillary windings. The specific search windings fitted to the machine have too few turns and are of thin wire so that the MMF is insufficient to affect the UMP. This was tested by injection of DC currents into both the main winding (5 A) and search coils (0.5 A). There was no detectable change in UMP.

However, there was good EMFs induced into these windings when the rotor was eccentric and this is studied later in the next chapter.

Chapter 4: Methodology and Experiment

4.1. Machine and Settings

For calculating the UMP, a new test rig is developed. A 4-pole wound rotor induction machine was utilized for this purpose. These machines are commonly used in wind turbine systems as generators. This machine is also known as Doubly Fed Induction Generator (DFIG) as both stator and rotor are separately connected to power supplies. The insulated winding of rotor of this machine is connected to external slips rings on the shaft via a WYE connection. The main specification in given in Appendix A and the winding diagram is shown in Appendix B

The main purpose of the slip rings is to provide resistance to rotor windings in series on starting for this particular machine. The main purpose of this resistance is to reduce starting current and increase torque in the state of rotor since it is a motor. The test rig is shown in Fig. 4.1.

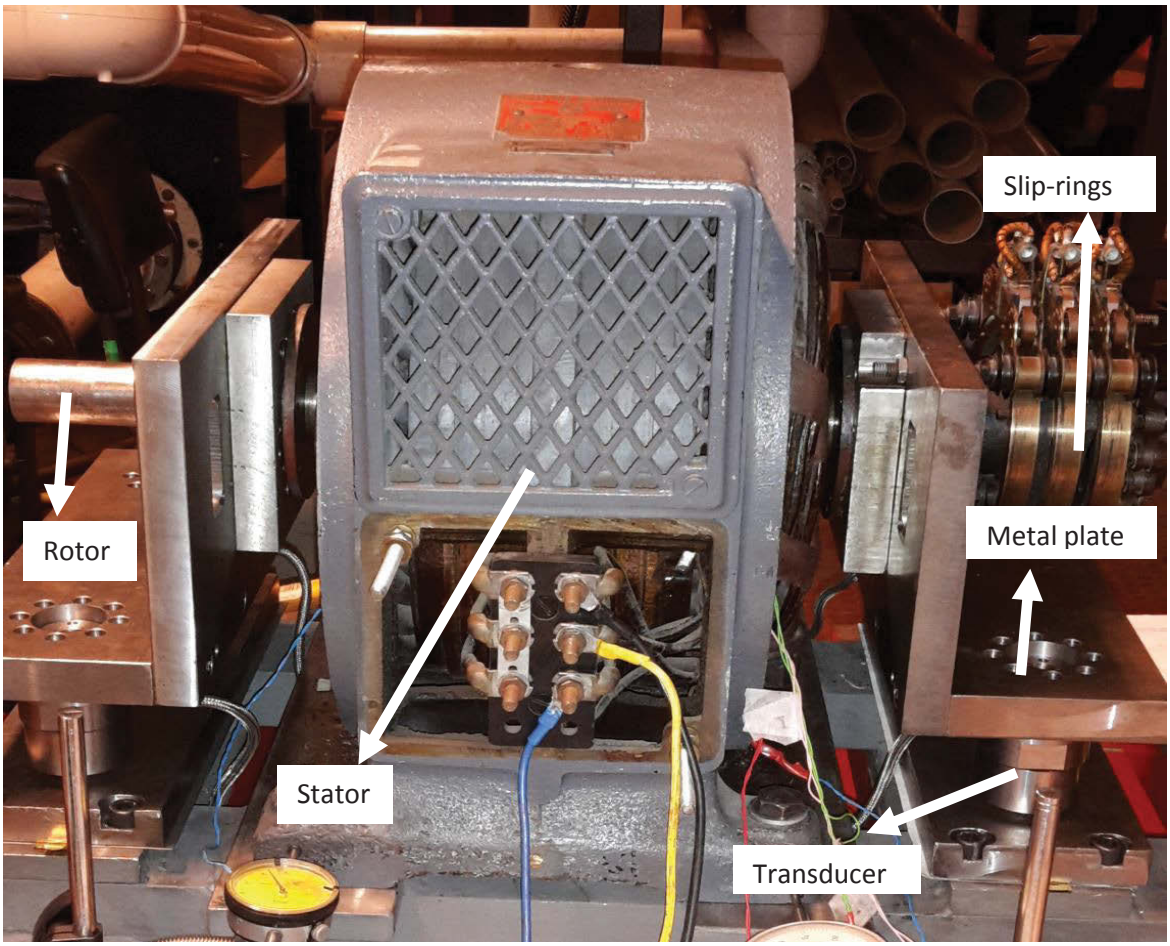

Figure 4.1: 4 Pole wound rotor induction machine

The machine rotor was set on a pair of metal plates and bolted tightly with the base to reduce the vibrations due to the motion of rotor. These metal plates support the rotor bearings of the Non Drive End (NDE) and drive End (DE). Within these rotor support structures are the piezo-electric force transducers which measure the UMP forces. The machine supports are shown in Figs. 4.2 and 4.3.

Figure 4.2: NDE of the motor

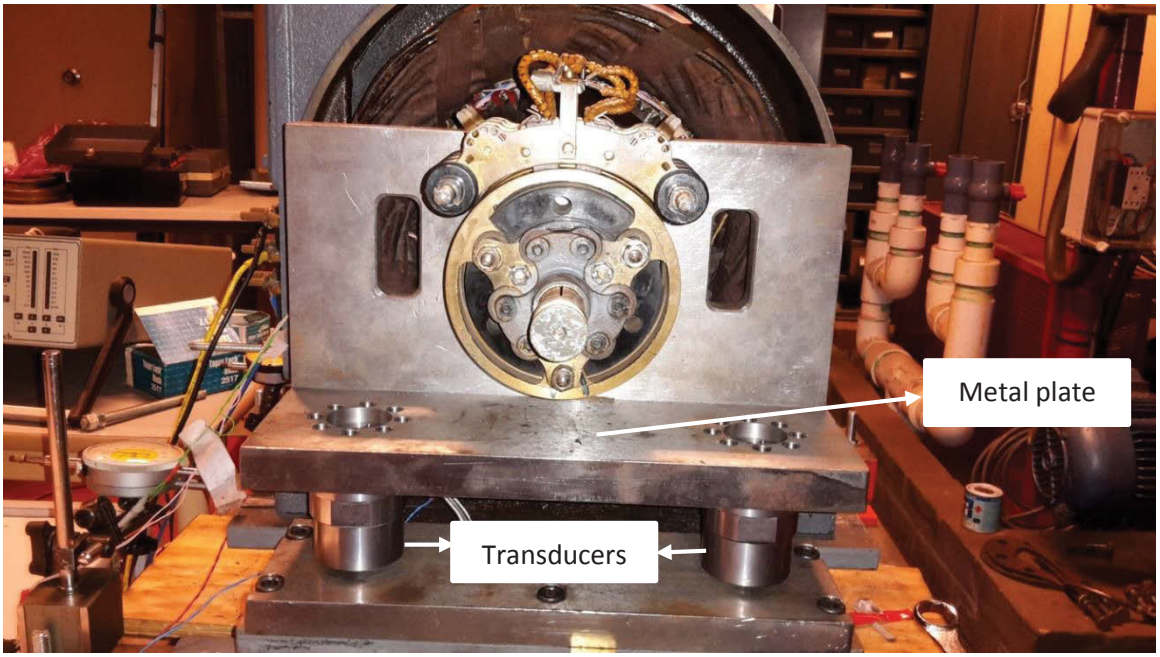

Figure 4.3: DE of the motor

The rotor of the motor is separately mounted on the plates which are helpful in positioning of the rotor and setting of air gap between rotor and stator during the experiment. This is shown clearly in Figs. 4.2 and 4.3.

A set of two transducers are mounted at each end of the rotor mounting on top of the metal plates as shown in Fig. 4.4. These transducers are used to measure the UMP and there are four of these in total.

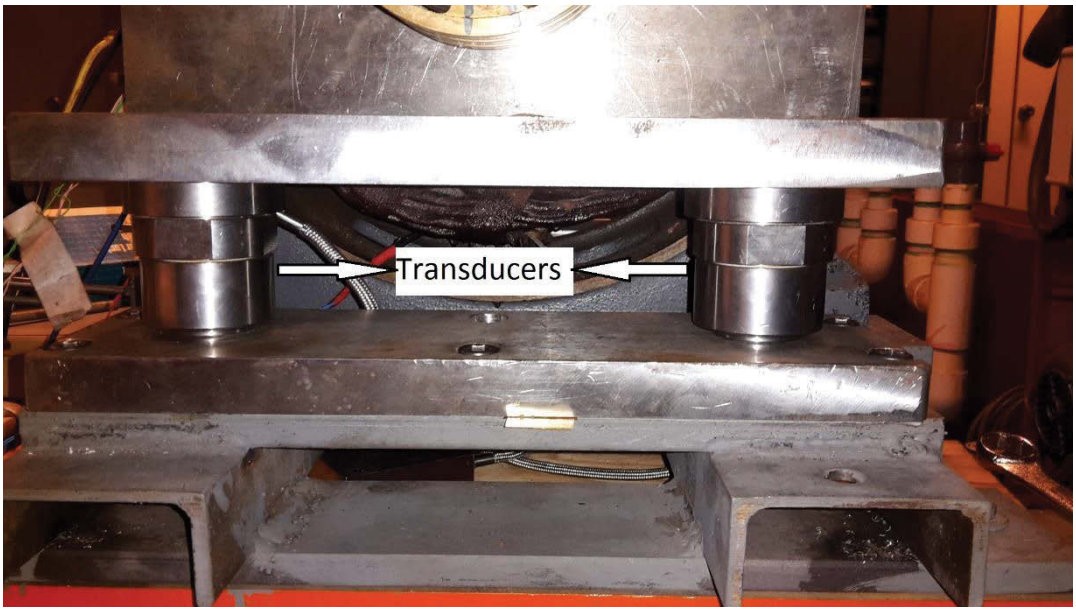

Figure 4.4: Transducers

Figure 4.5: Analyser

The radial forces that are generated are due to the UMP of the motor. For displaying the measured forces these transducers are connected to digital analyser, as shown in Figure 4.5.

For measuring the height and the air gap between the rotor and stator, clock gauges are used for this purpose.

The parameters of the motor are given in the Appendix A.

4.2. Transducers

Transducers are used to measure the active force regardless of point of action. A set of 4 sensors are used to measure forces in the experiment and each transducer consists of a 3-component force sensor which measures the force introduced through the top plate.

A pair of 3 quartz plates is used to measure the forces in the x, y and z directions. In each sensor, positive and negative charge appear at the connections depending upon the direction of force applied. Positive charge gives negative voltage at the output of the charge amplifies and vice versa. Fig. 4.6 shows 3 component force sensors in each of the sensor.

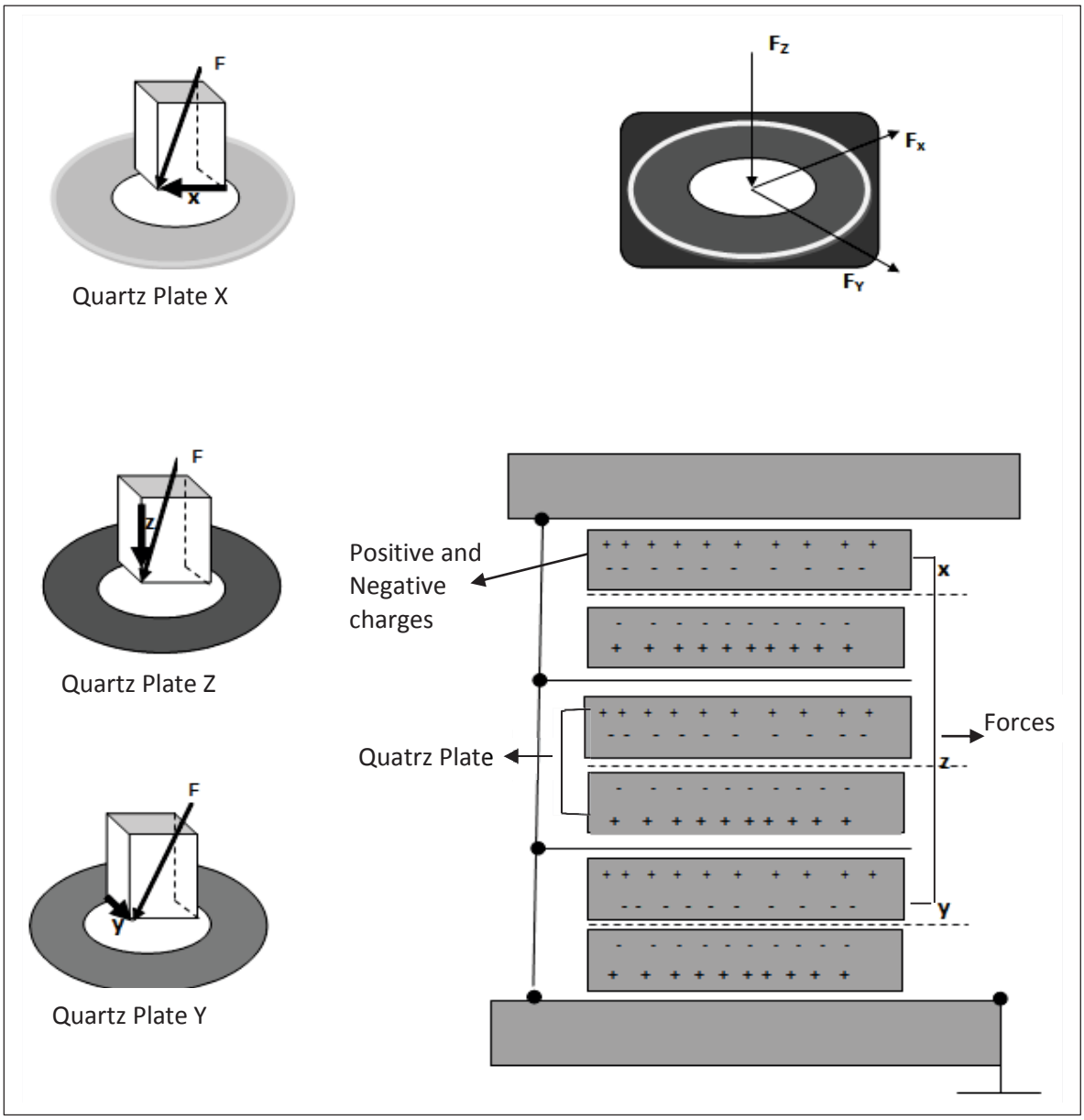

Figure 4.6: Component force Sensor

These sensors are connected to a summing box through integrated 3 wire cables. They are mounted under the metal plate on which the motor is mounted. Fig. 4.6 shows the placement of sensors on the test bed.

The summing box is connected to a multichannel change amplifier for measuring multicomponent force. It works on piezoelectric measurement concept, where sensors covert mechanical quantities into an electric charge. From the Fig. 4.7, it can be seen that the sensors are placed in parallel to measure the entire acting force.

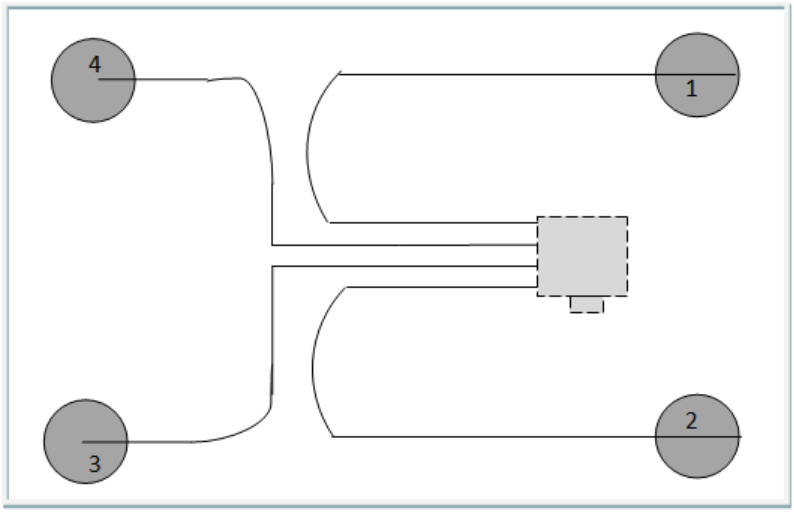

Figure 4.7: Sensors position

The eight channel charge amplifier calculates the forces on each channel as follows

$$\text{Channel 1} = F_{x1+2} \tag{4.1}$$

$$\text{Channel 2} = F_{x3+4} \tag{4.2}$$

$$\text{Channel 3} = F_{y1+4} \tag{4.3}$$

$$\text{Channel 4} = F_{y2+3} \tag{4.4}$$

$$\text{Channel 5} = F_{z1} \tag{4.5}$$

$$\text{Channel 6} = F_{z2} \tag{4.6}$$

$$\text{Channel 7} = F_{z3} \tag{4.7}$$

$$\text{Channel 8} = F_{z4} \tag{4.8}$$

To formulate calculations following expressions are used:

$$F_x = F_{x1+2} + F_{x3+4} \tag{4.9}$$

$$F_y = F_{y1+4} + F_{x2+3} \tag{4.10}$$

$$F_z = F_{z1} + F_{z2} + F_{z3} + F_{z4} \tag{4.11}$$

The experimental work is carried out to determine UMP in the machine and to reduce the UMP using different techniques of moving rotor eccentricity by changing rotor eccentricity in the DE and NDE. Only the x and z components are needed since the z measures the axial thrust.

4.3. Measurement of UMP

A 4 pole wound rotor induction machine is utilized to perform the experiments. This machine is set on a pair of metal plates and is bolted tightly with the plates bolted with the base; the reason of bolting it tightly with the base is to reduce vibrations in the machine in running condition. These both plates are set on the sides of the machine as shown in Figs. 4.7 and 4.8.

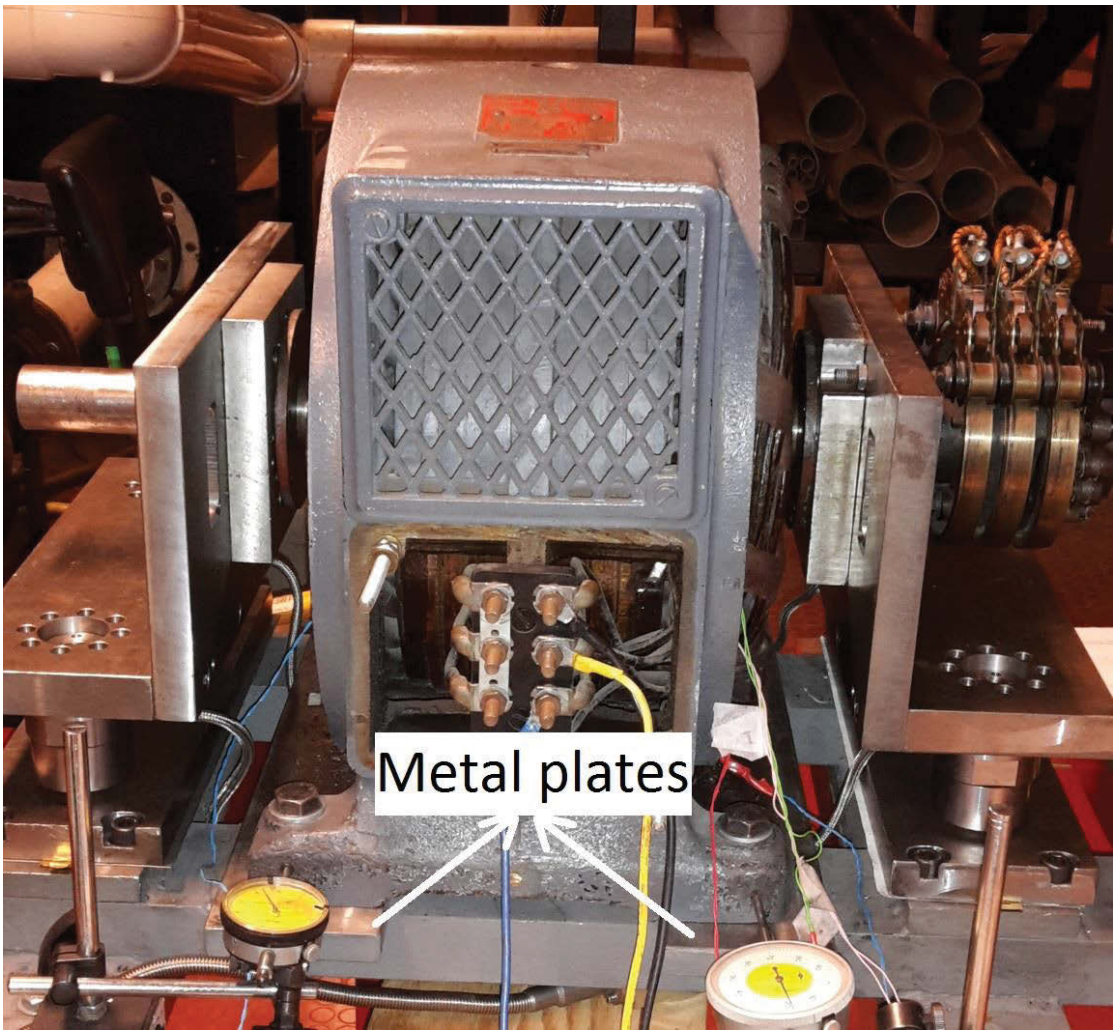

Figure 4.7: 1st side of machine.

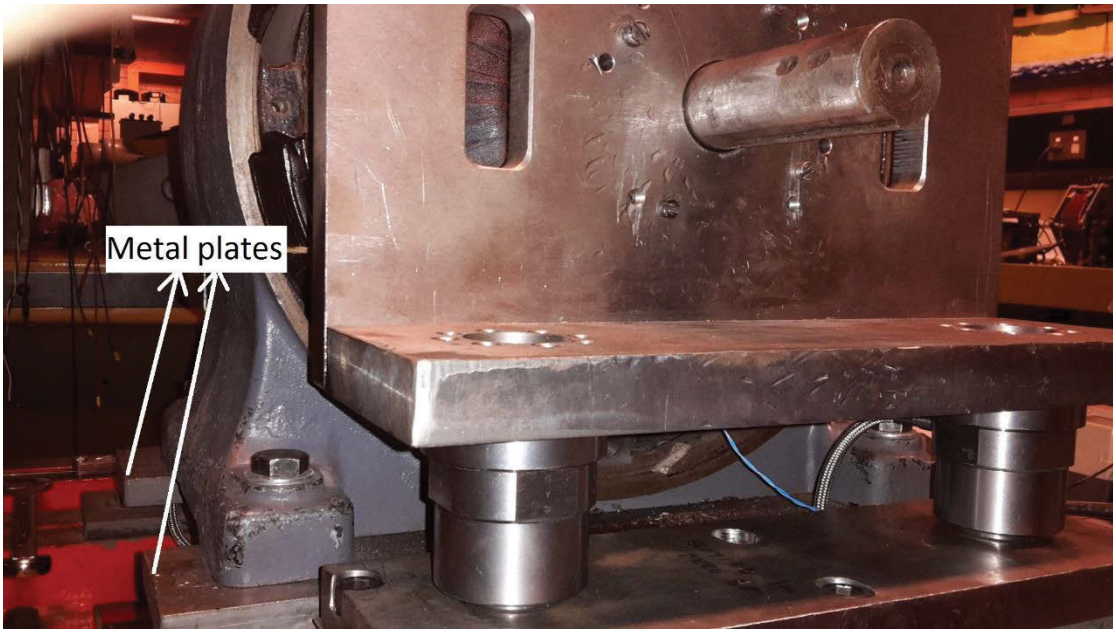

Figure 4.8: 2nd side of machine.

The rotor of the machine is separately mounted on plates, which helps in adjusting the height of the rotor with respect to the stator. This is dine using shims. The end of the machine with sliprings and carbon brushes is named as Non-Drive End (NDE) and the end with machine with the drive shaft is named as Drive End (DE). The piezoelectric transducers are set under the metal plates mounting rotor on DE and NDE, as shown in Fig. 4.4. The machine is then excited and the connection of machine with an autotransformer as shown in Appendix E.

These transducers are used to measure UMP forces acting on the machine in the running state and are capable of measuring forces in the x, y and z directions. The forces are measured as follows F_{x12}, F_{z1} and F_{z2} for the DE and F_{x34}, F_{z3} and F_{z4} for the NDE. There are 3 channels for each end. Defining the distance between the vertices of the shaft axis to the centre of transducers as x and the length of the shaft axis from the height of transducers as y as shown in Fig. 4.9.

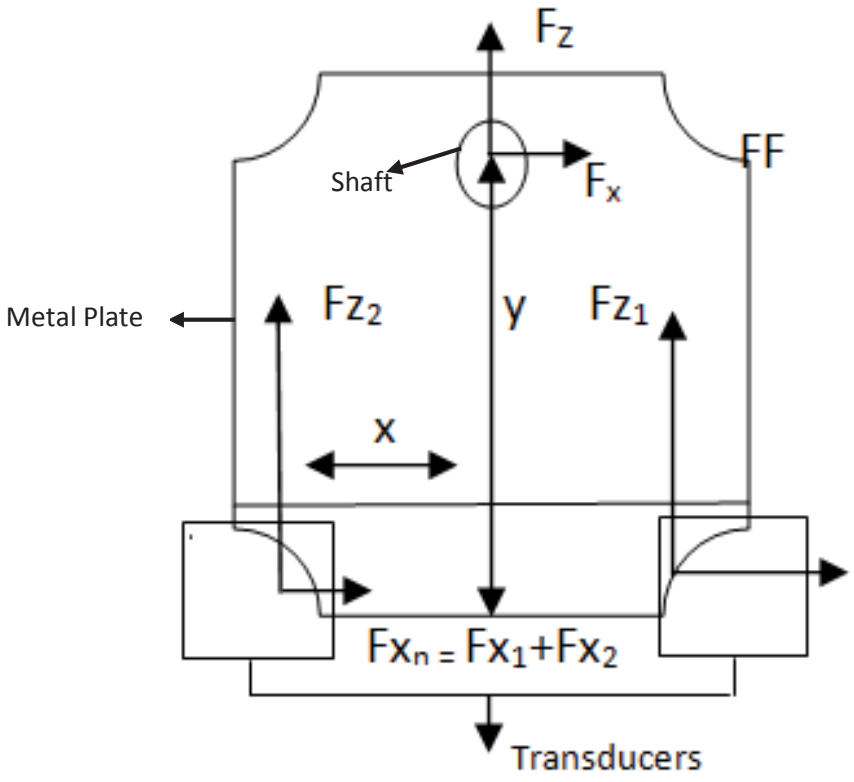

Figure 4.9: Test motor cofiguration

Then the vertical forces can be defined as:

$$F_{zT} = F_{z1} + F_{z2} + F_{z3} + F_{z4} \tag{4.12}$$

Considering the point of meeting where vertices from the shaft meet the horizontal line between the transducers, we can equate x and z in order to calculate the net x direction force:

$$F_{xT} = F_{x1} + F_{x2} \tag{4.13}$$

Since the z direction forces are tangential to x direction forces, then

$$F_{xT} = \tan(\theta) F_z \tag{4.14}$$

From Fig. 4.9 it can be seen that.

$$\tan\theta = {}^{x}/_{y} \tag{4.15}$$

So Eq. 4.14 becomes

$$F_{xT} = {}^{x}\!/_{y}\left(F_{z1} - F_{z2} - F_{z3} + F_{z4}\right) \tag{4.16}$$

The open circuit (running light test) and short circuit (locked rotor test) are performed to measure UMP of the machine. Under load conditions (locked rotor) UMP and torque exists together at the same time and can be separated depending on locking bar whether it is blocked against the rotor mounting and stator bed.

The torque expression is

$$T = Fd\sin\theta \tag{4.17}$$

$$T = F_{x1}\sin(\theta) + F_{x2}\sin(\theta) + (F_{z1} - F_{z2})\cos(\theta) + (F_{z4} - F_{z3})\cos(\theta) \tag{4.18}$$

While running a torque transducers can be used to separate torque and UMP in the machine. The normal air gap in an induction motors is usually small which makes it difficult to set and measure eccentricity.

The rotor and stator of the machine were not at the same height. In order to bring rotor and stator heights into alignment, the rotor mountings were shimmed with thin metal plates. These shim plates were measured to be 0.35 mm using Vernier callipers. Adjusting the height of the rotor also sets the air gap between rotor and stator. The air gap between the stator and rotor was measured using clock gauges. This is a trial and error method used after the rotor was nominally centred. This was done my minimizing the UMP of the machine. The air gap was continuously measured using clock gauges. When setting the centre positon, a number of trial fittings was done until it was nominally centred with an air gap length of 0.55 mm.

The motor is tested under open circuit test and short circuit test to obtain the UMP.

4.3.1. Open Circuit Test

The rotor of the motor is mounted on the shaft and the centre line of the shaft does not coincide with the centre of the mass. A centrifugal forces is produced when the shaft rotates and this force bends the shaft towards the centre of eccentricity of the mass. This causes the initial eccentricity of the rotor in a machine. The rotor was nominally centred with a 0.55mm air gap. By the help of shims to level the rotor, it was found that the rotor had 4% (0.04 x 0.55 = 0.022mm) eccentric at the start of the test which makes rotor centred with 0.57 mm air gap. The machine was then excited and forces are tabulated in Table 4.1. The force was measured

at different voltages from 0 to 240V using an autotransformer. The rotor was open-circuit and this is effectively equivalent to the running light test in a cage induction motor.

Table 4.1: Rotor nominally centred.

V	I	FX12	FX34	FY14	FY23	FZ1	FZ2	FZ3	FZ4	εFZ
50	0.754	3	5	0	0	1	-3	-4	2	-4
100	1.4	16	21	-1	3	6	-15	-18	11	-16
150	2.1	36	47	-2	6	15	-34	-39	24	-34
200	2.9	57	74	-1	10	25	-53	-62	38	-52
240	3.78	62	77	-2	12	31	-60	-65	42	-52

The rotor was then moved from 4 % eccentricity to 20 % eccentric position (nominal); the eccentricity was found to be 14 %. The forces were again tabulated with voltage variation as shown in Table 4.2.

Table 4.2: 20 % eccentric position of rotor.

V	I	FX12	FX34	FY14	FY23	FZ1	FZ2	FZ3	FZ4	εFZ
50	0. 714	-17	-18	2	-2	-13	10	9	-15	-9
100	1.36	-74	-72	2	-1	-57	42	38	-56	-33
150	2.05	-166	-163	5	-3	-130	94	86	-129	-79
200	2.83	-250	-244	5	0	-195	140	131	-195	-119
240	3.66	-265	-260	8	2	-204	148	140	-204	-120

Now the rotor is moved to the 40 % eccentricity position and it was found to be 30% eccentric. The results are tabulated in Table 4.3.

Table 4.3: 30 % eccentric position of the rotor.

V	I	FX12	FX34	FY14	FY23	FZ1	FZ2	FZ3	Fz4	εFZ
50	0. 683	-39	-40	2	-2	-27	24	24	-28	-7
100	1.31	-165	-170	8	-8	-119	105	102	-123	-35
150	1.96	-362	-360	6	-6	-260	228	218	-262	-76
200	2.791	-530	-525	3	-1	-384	332	317	-381	-116
240	3.7	-570	-560	4	2	-410	354	345	-410	-121

These measured forces were then matched with the results obtained using Finite Element Analysis (FEA). This was done to adjust the position from the approximate nominal positions set with the clock gauges. It was found that measured UMP was nearly matched with the FEA results as shown in Figure 4.10.

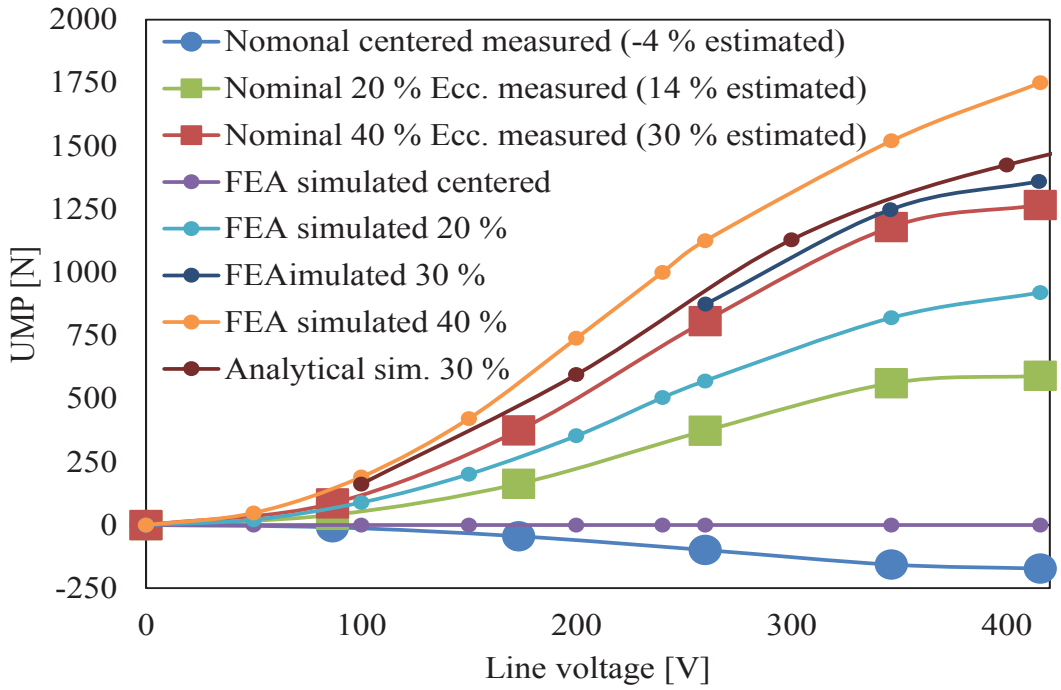

Figure 4.10: Open circuit UMP measurement results.

These results show that an increase in UMP occurs as voltage increases. This is verified with the theory of the machine when voltage is applied to the rotor displacements it gives rise to UMP. However, as the voltage approaches the rated value of the machine then it levels out as the core starts to saturate.

4.3.2. Short Circuit Test:

The rotor bar is locked using a locking bar as shown in Figure 4.11 to perform the experiment.

Figure 4.11: rotor with locking bar.

The machine was then excited and several results were obtained when rotor was short circuited at the slip rings. These measured results again matched well the simulated analytical results. For the skewed analytical simulation, the measured UMP is significantly higher than the un-skewed simulations at all eccentricities. The skew increases the UMP as discussed in [64]. There is an axial saturation and damping effect on UMP due to the skew on the rotor. The flux levels will change along the axial length since the phase angle between the stator and rotor flux waves will vary down the axial length of the machine [66].

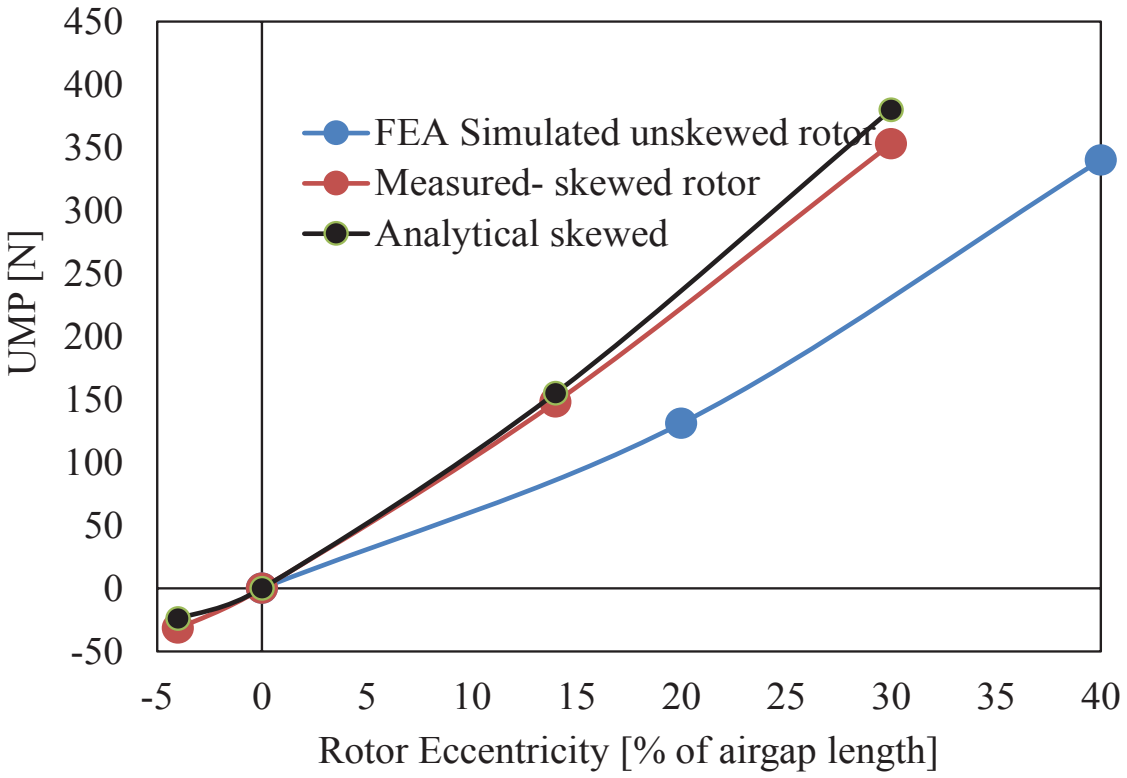

Figure 4.12: Short circuit locked rotor UMP measurements.

When the machine was tested rotor with a locking bar, torque was obtained by measurements. Torque was extracted from the force measurements when rotor was locked with a locking bar against the stator bed. The test was performed with V_{ph} = 48 V and line current I_{line} = 11.1 A and 11.85 A simulated. The torque was 5.1 Nm measured and 4 Nm simulated. It was found that the correlation reasonable for a locked rotor test. This torque can be difficult to predict and the difference is probably partly due to the skew which increases the effective rotor resistance.

The tests were also performed with changing rotor positions at the DE and NDE. First the rotor position was changed at the DE to 40 % eccentricity with the NDE kept at nominally centred eccentricity. It was repeated again with the NDE position changed to 40 % eccentricity and the DE kept nominally centred. It was found the changed position end had higher force acting on it in both cases as shown in Figure 4.13.

The net force on the rotor in this test is no longer at the axial centre as one end of the rotor is not centred. The end with eccentricity will experience more force than the end which is centred positioned. This was also performed with open circuit light running test and the results are shown in Figure 4.16.

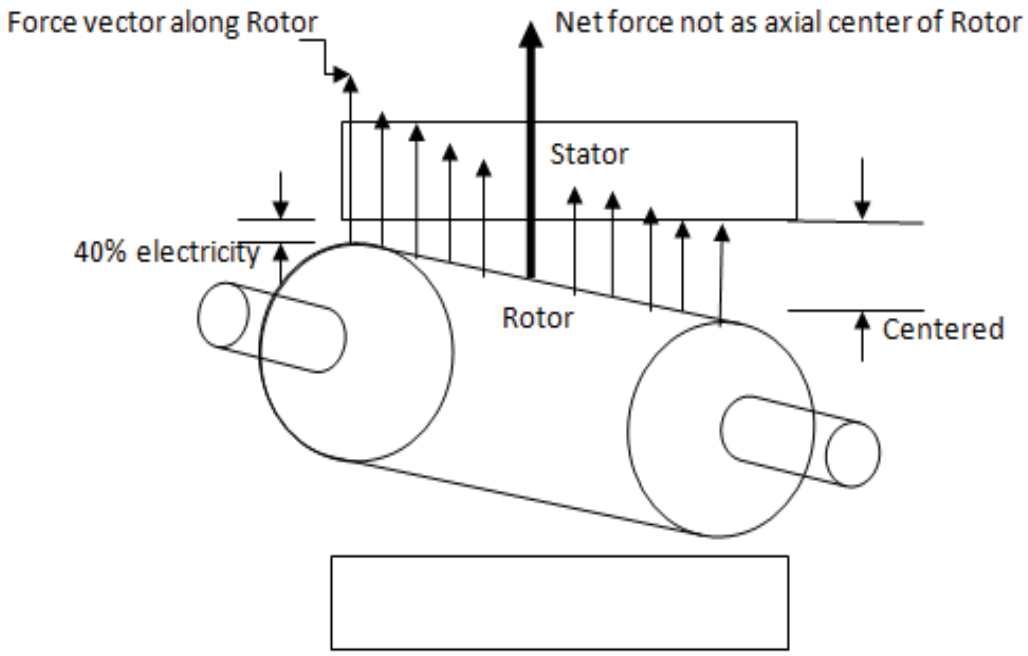

Figure 4.13: Effects of axial variation of eccentricity on the UMP.

Table 4.4: NDE moved 40 % while DE centred.

V	I	FX12	FX34	FY14	FY23	FZ1	FZ2	FZ3	FZ4	εFZ
50	0.719	36	33	3	-2	27	-22	-21	25	9
100	1.36	150	137	12	-6	111	-91	-84	103	39
150	2.046	326	305	19	-6	240	-200	-187	237	90
200	2.897	482	457	28	-5	360	-297	-273	349	139
240	3.82	524	493	41	-7	392	-321	-301	370	140

Table 4.5: DE moved 40 % while NDE centred.

V	I	FX12	FX34	FY14	FY23	FZ1	FZ2	FZ3	FZ4	εFZ
50	0.708	34	37	0	0	24	-21	-24	28	7
100	1.35	144	154	4	1	106	-89	-97	115	35
150	2.05	320	346	4	7	235	-199	-217	258	77
200	2.9	473	507	8	13	351	-294	-316	380	121
240	3.85	509	543	15	16	374	-321	-339	406	120

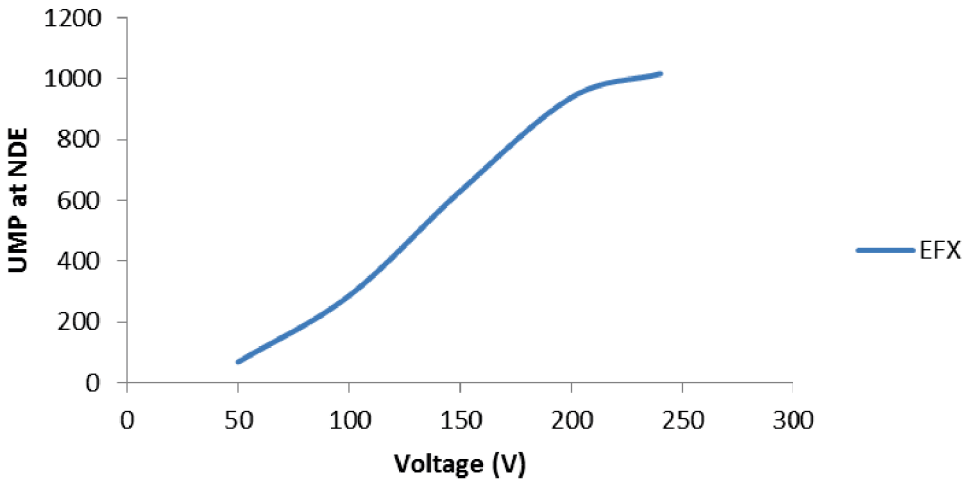

Figure 4.14: NDE moved 40% while DE centred.

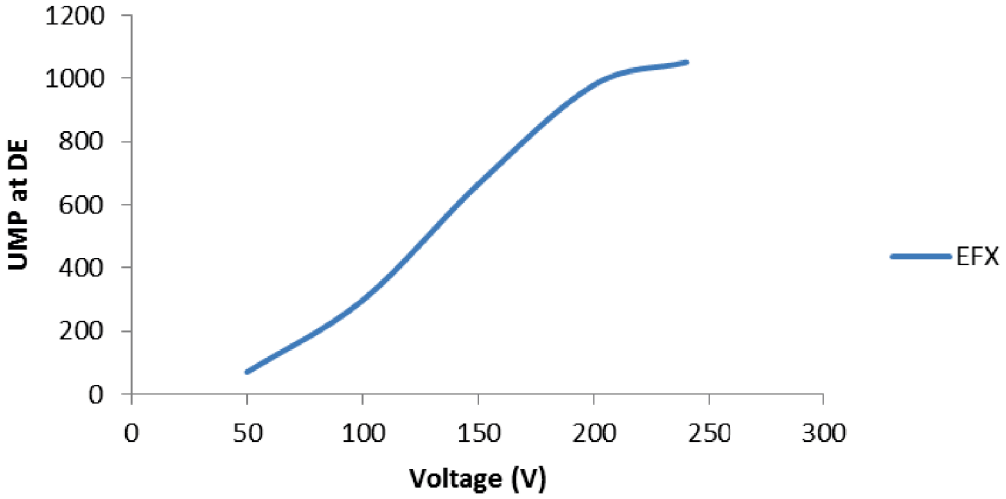

Figure 4.15: DE moved 40% while NDE centred.

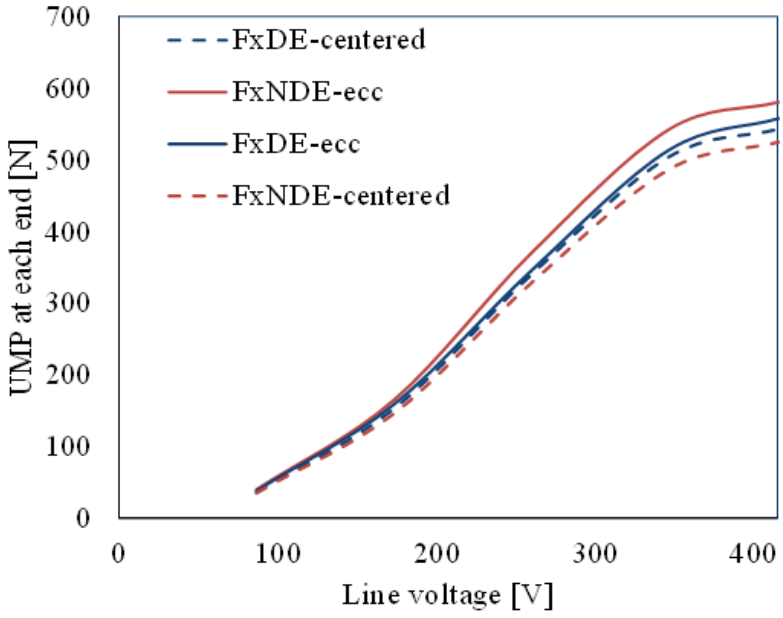

Figure 4.16: Axial variation of eccentricity.

From the results it is clear that as the voltage keeps on increasing, the UMP also increases. Although a linear behaviour is seen in the UMP when the DE is centred and the NDE is eccentric, and when the NDE is centred and the DE is eccentric

4.4. 2 Pole and 6 Pole Search Winding

The motor was modified with different types of search coil. It was modified with 6-pole and 2-pole specific search windings as shown in Fig. 4.17.

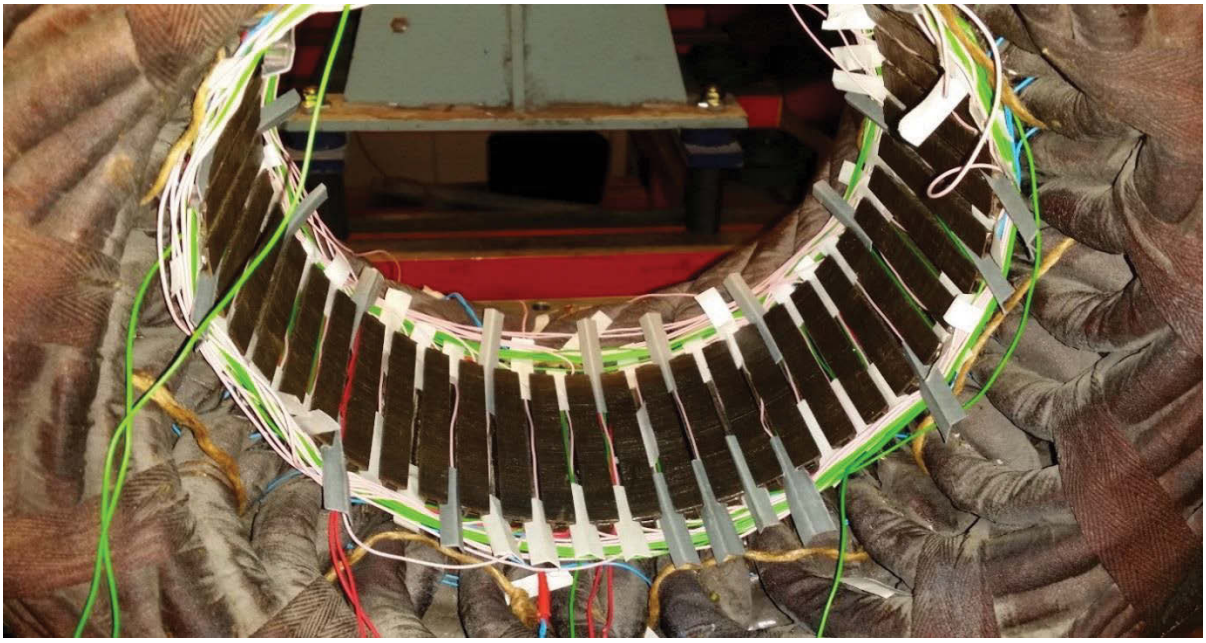

Figure 4.17: 2 pole and 6 pole Winding

The rotor of the machine was refitted as previously and mounted on pedestals that includes piezo-electric force transducers to measure direct UMP on each bearing. The motor was tested again with open circuit, and rotor short circuit with locked rotor.

Initially only the 6-pole search winding (as shown in Appendix D) was implemented and tested. The motor was then tested with varying eccentricities (40 %, 60 % and 5 %) and the voltage in the 6 pole winding was measured. Table 4.6 presents the results that were obtained from the open circuit and short circuit tests.

Table 4.6: Short circuit and open circuit with 6 pole winding.

Centred 0.55 mm airgap									
Short Circuit (50V, 4.2 A)									
	6-pole V	**FX12**	**FX34**	**FY14**	**FY23**	**FZ1**	**FZ2**	**FZ3**	**FZ4**
Read 1	456mV	-9	-2	-1	0	0	4	2	3
Read 2	456mV	-5	-2	-1	0	0	4	3	3
Open Circuit (200V, 0.93 A)									
	6-pole V	**FX12**	**FX34**	**FY14**	**FY23**	**FZ1**	**FZ2**	**FZ3**	**FZ4**
Read 1	1.6V	-10	-1	1	1	27	28	28	34
Read 2	1.6V	-10	-1	2	1	28	28	28	34
At 0.4 mm min airgap eccentricity (40 %)									
Short Circuit (50V, 4 A)									
	6-pole V	**FX12**	**FX34**	**FY14**	**FY23**	**FZ1**	**FZ2**	**FZ3**	**FZ4**
Read 1	576mV	6	11	-2	2	-10	16	13	-6
Read 2	568mV	6	12	-1	1	-10	16	14	-6
Open Circuit (200V,0.91 A)									
	6-pole V	**FX12**	**FX34**	**FY14**	**FY23**	**FZ1**	**FZ2**	**FZ3**	**FZ4**
Read 1	3.36V	100	102	2	5	-51	116	114	-40
Read 2	3.36V	103	104	2	4	-52	118	116	-42
At 0.2 mm min air gap eccentricity (60 %)									
Short Circuit (50V, 4 A)									
	6-pole V	**FX12**	**FX34**	**FY14**	**FY23**	**FZ1**	**FZ2**	**FZ3**	**FZ4**
Read 1	1.48V	55	68	-2	3	-48	60	60	-47
Read 2	1.48V	63	64	-1	3	-48	61	58	-42
Open Circuit (200V, 0.78 A)									
	6-pole V	**FX12**	**FX34**	**FY14**	**FY23**	**FZ1**	**FZ2**	**FZ3**	**FZ4**
Read 1	10.2V	290	370	55	-28	-194	280	329	-242
Read 2	10.2V	300	356	32	-11	-199	276	317	-227

The Figure 4.18 shows the characteristics of the UMP as it varies with eccentricity. There is a degree of eccentricity variation down the axial length of machine and the degree of eccentricity is not precise.

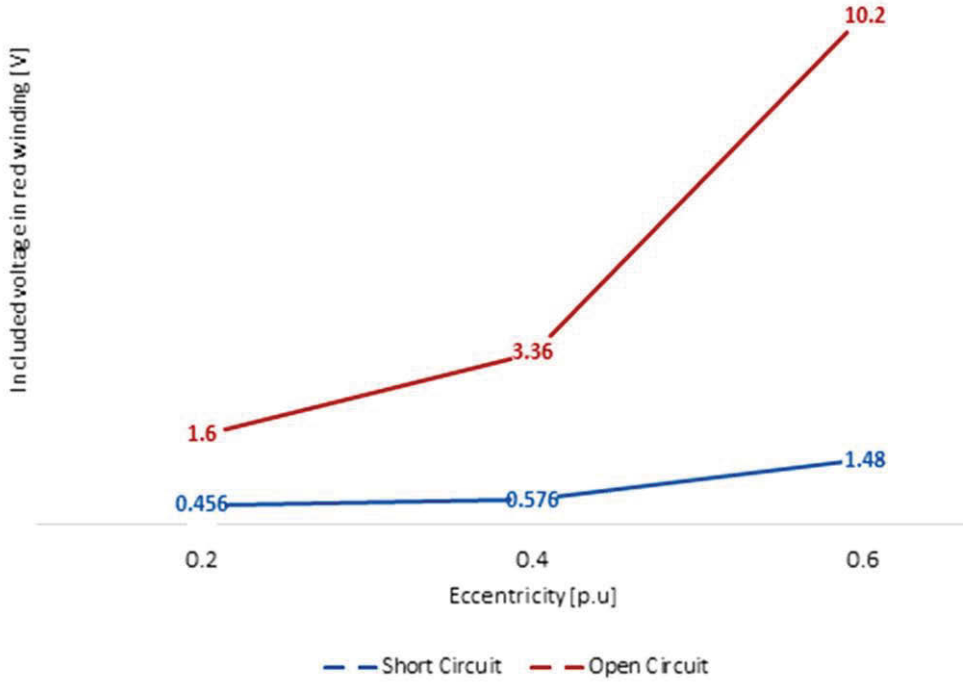

Figure 4.18: 6 pole results with open circuit and locked rotor.

For further experiments, the machine was dismantled and 2-pole search windings were inserted (as shown in Appendix C) on quadrature axes (α and β). The results show linear characteristics. The eccentricity was less in this test. The short circuit test was done at 50 V and if linearity is assumed, then these results should be four times less but the induction motor demagnetizes as it is loaded and results in UMP. The open circuit test voltages for the 2-poles windings are shown in Fig. 4.19. It can been seen that it has a linear characteristic. The voltages for 2-pole winding are higher. The 2 pole voltages should be scaled by 3/2 with respect to the 6-pole voltages when considering the number of search winding turns and the analysis in the previosu chapter. This approximately holds. The voltages in the 2-pole windings were investigated and found to be 90 degrees out of phase. This is expected.

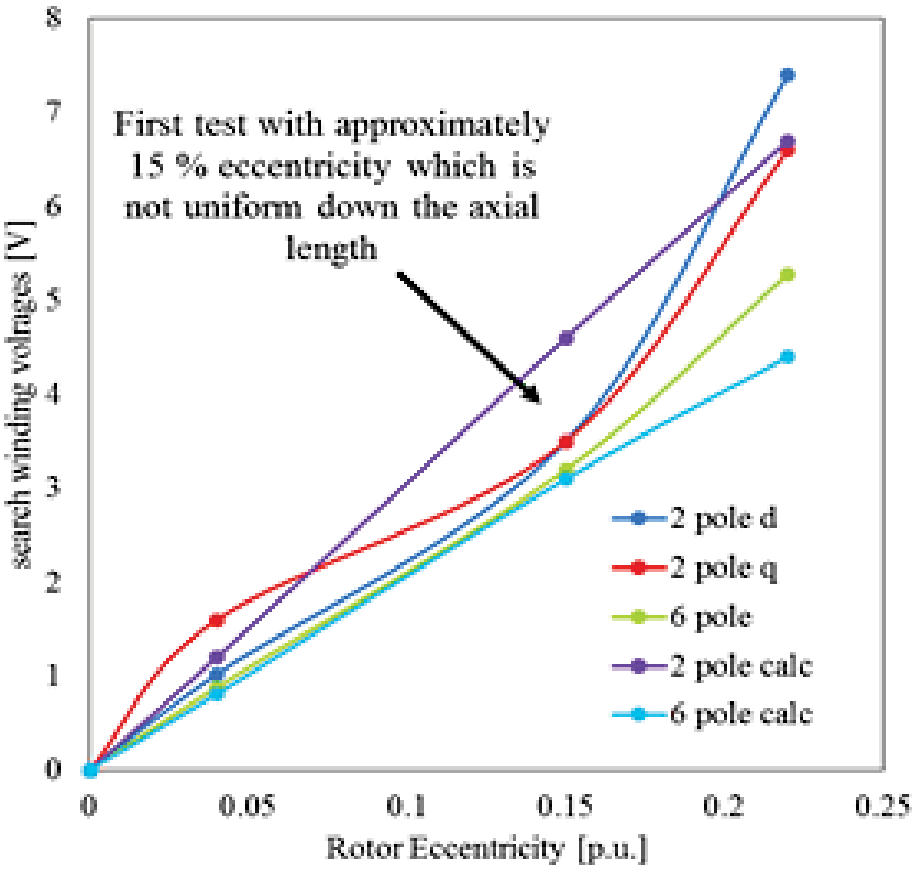

Figure 4.19: 2 pole winding tests.

The results in Tables 4.7 to 4.12 show results from non-uniform eccentricity in the machine. The test started with 40 % eccentricity at one end and the rotor is then moved one end at time to reduce the eccentricity. As average eccentricity is reduced, the UMP and search coil voltages are also reduced. This illustrates that even with non-constant eccentricity, the search coil detection methods can be used to predict eccentricity. The search coils were open circuit and the voltages measured. They were also shorted and a current was induced into them. Fig 4.26 gives the raw UMP data for farces ate each end of the machine.

From the comparison between UMP with different rotor eccentricities in Fig. 4.27 it is clearly noticed that the UMP of the machine reduces with the rotor eccentricity pattern that is followed. This evaluates that eccentricity plays a vital role in the reduction of UMP in the machine.

Similarly Fig. 4.28 is a comparison between the voltages of the search coil windings and the UMP of the machine. When following the same pattern of the rotor eccentricities, the results are in a descending order of voltages in the search coil windings.

These results provides evidence for the relationship between the UMP with the voltages in the search coil windings. The UMP in the machine decreases with the fall in the voltages of the search coil windings with the changing eccentricities in the rotor.

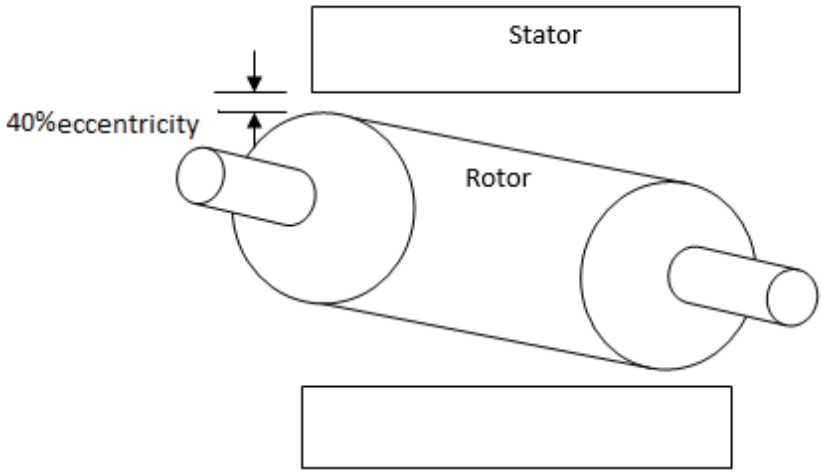

Figure 4.20: DE 40 % Eccentric

Table 4.7: DE 40 % Eccentric

Short Circuit (50 V, 3.5 A)											
	2-pole V_2	**2-pole V_1**	**6-pole V**	**FX12**	**FX34**	**FY14**	**FY23**	**FZ1**	**FZ2**	**FZ3**	**FZ4**
Read 1	1.8mV	1.3V	880mV	-50	-21	5	-5	37	-36	-46	34
(A2 = 14 mA, A1 = 11 mA)											
Read 2 after short circuited 2-pole windings, and the Ammeter reading 23 mA											
				-47	-20	-5	-4	28	-32	-36	24
Read 3 after shorting 2-pole windings at 121.19 V, 9.5 A with current 74 mA (A2=45 mA , A1=51 mA)											
				-269	-105	20	-21	171	-230	-235	174
Open Circuit (200 V, 0.902 A)											
	2-pole V_2	**2-pole V_1**	**6-pole V**	**FX12**	**FX34**	**FY14**	**FY23**	**FZ1**	**FZ2**	**FZ3**	**FZ4**
Read 1	4.6V	5.6V	5V	-131	-45	9	-13	101	-106	-106	102
Read 2 after short circuited 2-pole windings, and the Ammeter reading 82 mA (A2=42 mA, A1=37 mA)											
				-141	-55	12	-9	102	-104	-111	104

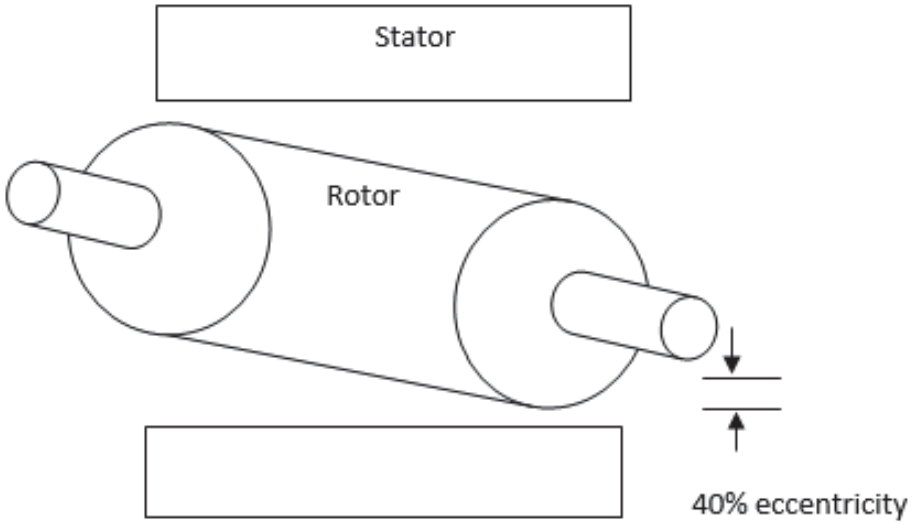

Figure 4.21: NDE 40 % Eccentric

Table 4.8: NDE 40 % Eccentric.

Short Circuit (50 V, 3.5 A)											
	2-pole V_2	**2-pole V_1**	**6-pole V**	**FX12**	**FX34**	**FY14**	**FY23**	**FZ1**	**FZ2**	**FZ3**	**FZ4**
Read 1	680 mV	1.16V	1.12V	39	14	-6	4	-41	24	20	-33
(A2= 4 mA, A1= 16 mA)											
Read 2 after short circuited 2-pole windings, and the Ammeter reading 14 mA											
				35	13	-5	5	-43	22	22	-31
Read 3 after shorting 2-pole windings at 124 V, 9.91 A with current 35 mA (A2=32 mA , A1=14 mA)											
				193	69	-16	12	-194	97	101	-170
Open Circuit (200 V, 0.908 A)											
	2-pole V_2	**2-pole V_1**	**6-pole V**	**FX12**	**FX34**	**FY14**	**FY23**	**FZ1**	**FZ2**	**FZ3**	**FZ4**
Read 1	3.52V	5.2V	4.4V	105	36	-12	11	-99	60	55	-93
Read 2 after short circuited 2-pole windings, and the Ammeter reading 85 mA (A2=63 mA, A1=52 mA)											
				81	30	-8	10	-90	42	41	-83

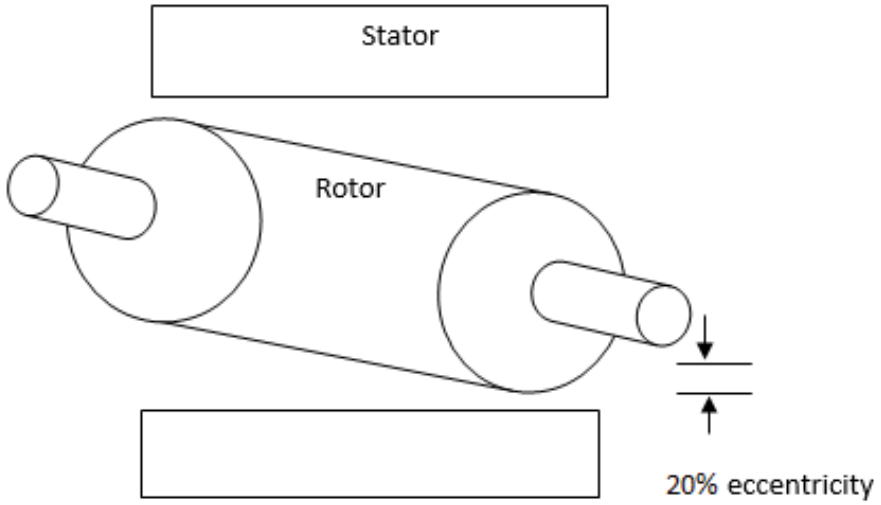

Figure 4.22: NDE 20 % Eccentric

Table 4.9: NDE 20 % Eccentric.

Short Circuit (50 V,3.51 A)											
	2-pole V_2	**2-pole V_1**	**6-pole V**	**FX12**	**FX34**	**FY14**	**FY23**	**FZ1**	**FZ2**	**FZ3**	**FZ4**
Read 1	780mV	540mV	480 mV	8	1	-5	3	-16	6	2	-11
(A2= 7 mA, A1= 3 mA)											
Read 2 after short circuited 2-pole windings, and the Ammeter reading 10 mA											
				7	2	-1	0	-11	1	2	-8
Read 3 after shorting 2-pole windings at 125.5 V, 9.62 A with current 35 mA (A2=23 mA , A1=9 mA)											
				39	12	-2	3	-47	-4	2	-42
Open Circuit (200 V,0 .92 A)											
	2-pole V_2	**2-pole V_1**	**6-pole V**	**FX12**	**FX34**	**FY14**	**FY23**	**FZ1**	**FZ2**	**FZ3**	**FZ4**
Read 1	1.44V	1.44V	1.2V	24	7	-2	3	-34	6	3	-25
Read 2 after short circuited 2-pole windings, and the Ammeter reading 14 mA (A2=14 mA, A1=10 mA)											
				19	6	-2	3	-32	5	2	-22

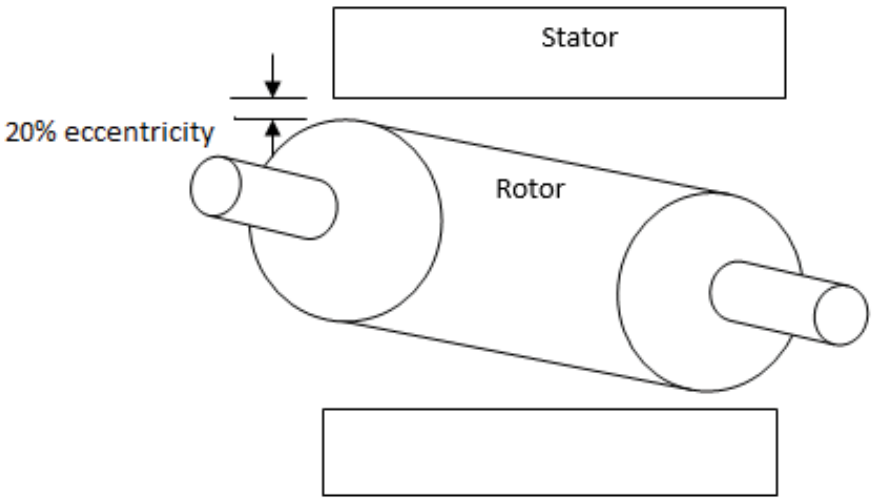

Figure 4.23: DE 20 % Eccentric

Table 4.10: DE 20 % Eccentric.

Short Circuit (50 V, 3.52 A)											
	2-pole V_2	**2-pole V_1**	**6-pole V**	**FX12**	**FX34**	**FY14**	**FY23**	**FZ1**	**FZ2**	**FZ3**	**FZ4**
Read 1	1.10mV	720mV	312mV	-12	-6	-2	-4	0	-6	-6	1
(A2= 5 mA, A1= 3 mA)											
Read 2 after short circuited 2-pole windings, and the Ammeter reading 10 mA											
				-11	-5	3	-3	3	-11	-8	2
Read 3 after shorting 2 pole windings at 123 V, 9.7 A with current 39 mA (A2=20 mA , A1=15 mA)											
				37	-20	-1	0	13	-55	-57	20
Open Circuit (200 V, 0.92 A)											
	2-pole V_2	**2-pole V_1**	**6-pole V**	**FX12**	**FX34**	**FY14**	**FY23**	**FZ1**	**FZ2**	**FZ3**	**FZ4**
Read 1	1.56V	1.12V	1.1V	-18	-9	1	-1	1	-25	-26	8
Read 2 after short circuited 2-pole windings, and the Ammeter reading 22 mA (A2=16 mA, A1=9 mA)											
				-20	11	1	0	2	-24	-30	11

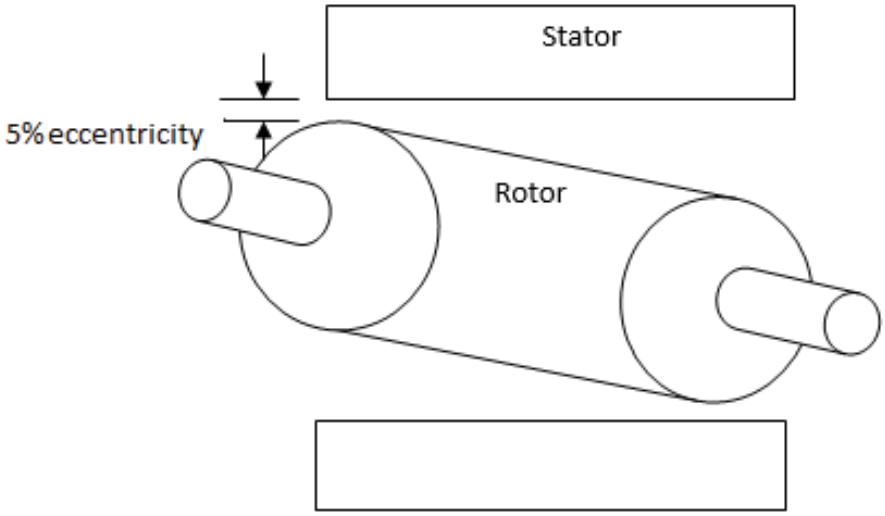

Figure 4.24: DE 5 % Eccentric

Table 4.11: DE 5 % Eccentric.

Short Circuit (50 V, 3.51 A)											
	2-pole V_2	**2-pole V_1**	**6-pole V**	**FX12**	**FX34**	**FY14**	**FY23**	**FZ1**	**FZ2**	**FZ3**	**FZ4**
Read 1	960mV	500mV	624mV	17	6	1	0	-19	5	10	-19
(A2= 5 mA, A1= 2 mA)											
Read 2 after short circuited 2 pole windings, and the Ammeter reading 8 mA											
				15	6	0	1	-20	8	8	-16
Read 3 after shorting 2 pole windings at 121.33V,9.55A with current 24 mA (A2=25 mA , A1=9 mA)											
				71	26	-2	3	-70	21	32	-70
Open Circuit (200 V, 0.909 A)											
	2-pole V_2	**2-pole V_1**	**6-pole V**	**FX12**	**FX34**	**FY14**	**FY23**	**FZ1**	**FZ2**	**FZ3**	**FZ4**
Read 1	1.84V	2.16V	2V	49	16	-2	3	-56	20	20	-41
Read 2 after short circuited 2 pole windings, and the Ammeter reading 32 mA (A2=19 mA, A1=21 mA)											
				44	14	-3	3	-44	18	19	-41

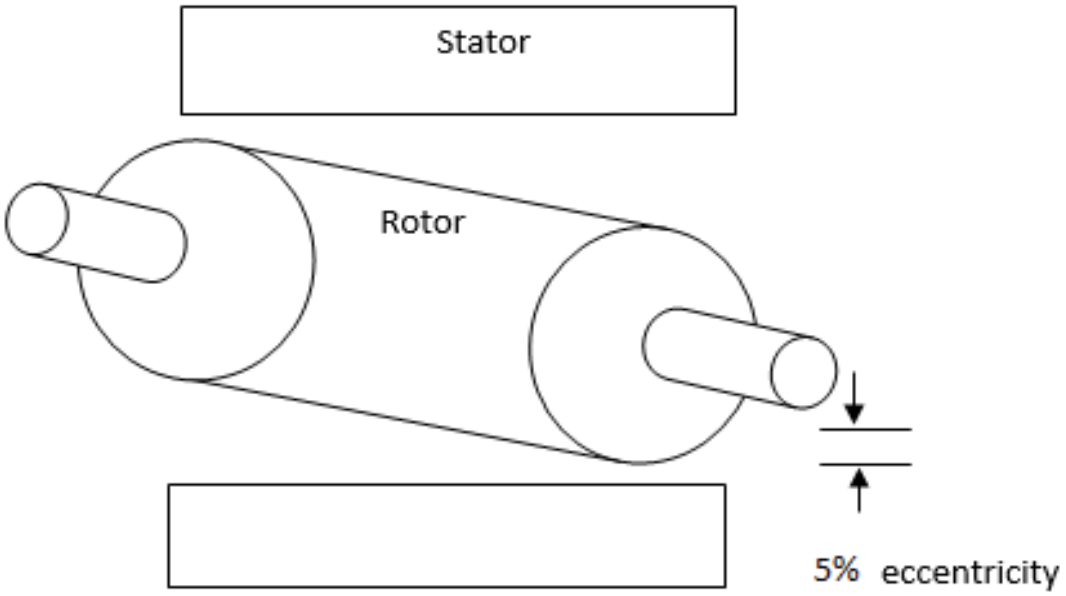

Figure 4.25: NDE 5 % Eccentric

Table 4.12: NDE 5 % Eccentric.

Short Circuit (50 V, 3.52 A)											
	2-pole V_2	**2-pole V_1**	**6-pole V**	**FX12**	**FX34**	**FY14**	**FY23**	**FZ1**	**FZ2**	**FZ3**	**FZ4**
Read 1	760mV	700mV	384mV	-3	-1	2	-5	-1	-5	-1	-1
(A2= 7mA, A1= 2mA)											
Read 2 after short circuited 2 pole windings, and the Ammeter reading 7mA											
				-3	-1	3	0	0	-1	-2	0
Read 3 after shorting 2 pole windings at 122.7 V, 9.7 A with current 52 mA (A2=32 mA , A1=20 mA)											
				-5	-3	4	-4	-14	-30	-22	-11
Open Circuit (200 V, 0.925 A)											
	2-pole V_2	**2-pole V_1**	**6-pole V**	**FX12**	**FX34**	**FY14**	**FY23**	**FZ1**	**FZ2**	**FZ3**	**FZ4**
Read 1	1.36V	760mV	760mV	49	16	-2	3	-56	20	20	-41
Read 2 after short circuited 2 pole windings, and the Ammeter reading 18 mA (A2=13 mA, A1=8 mA)											
				3	0	2	1	-15	-8	-9	-8

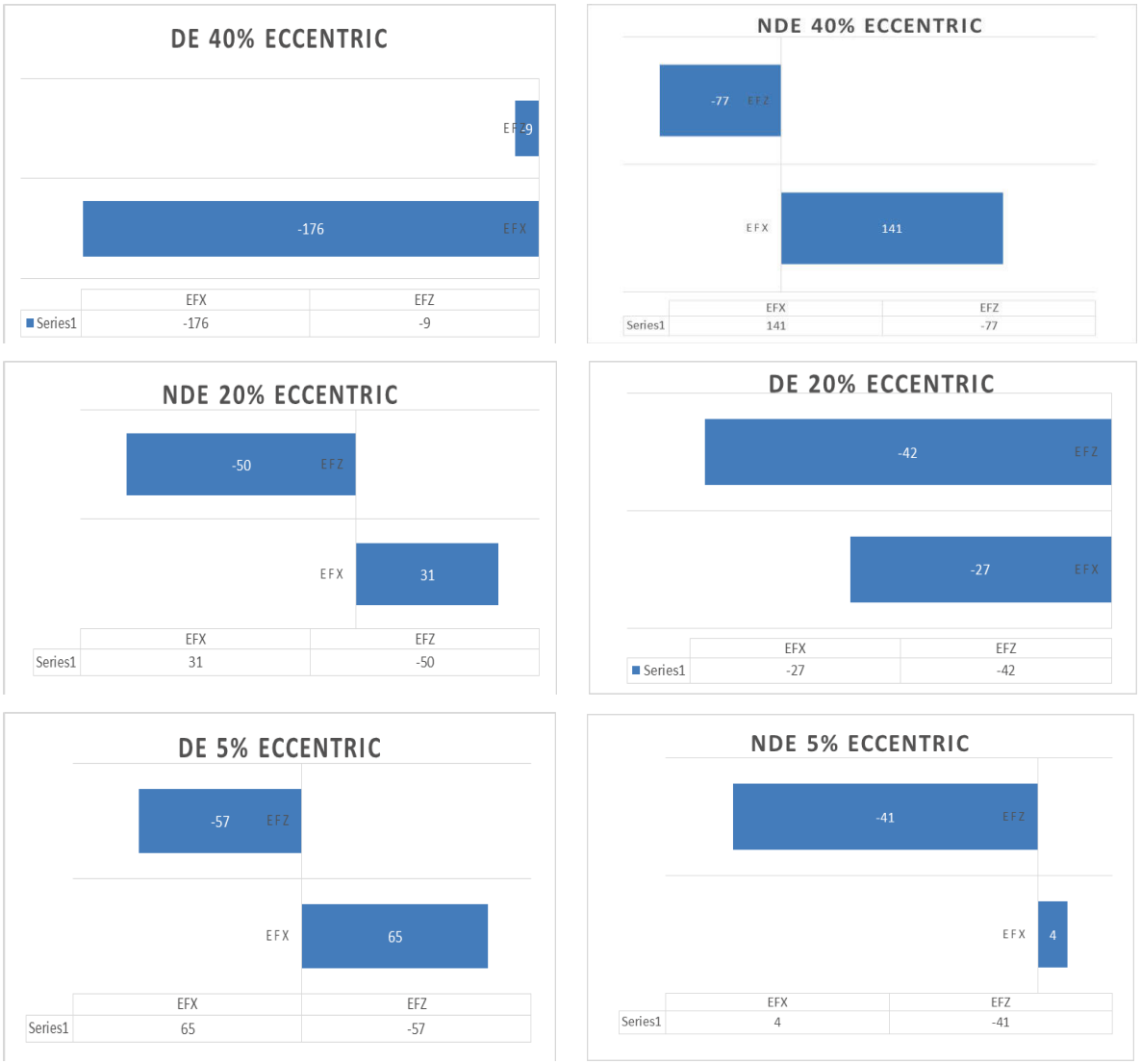

Figure 4.26: Results of Different rotor eccentricities as the rotor is moved.

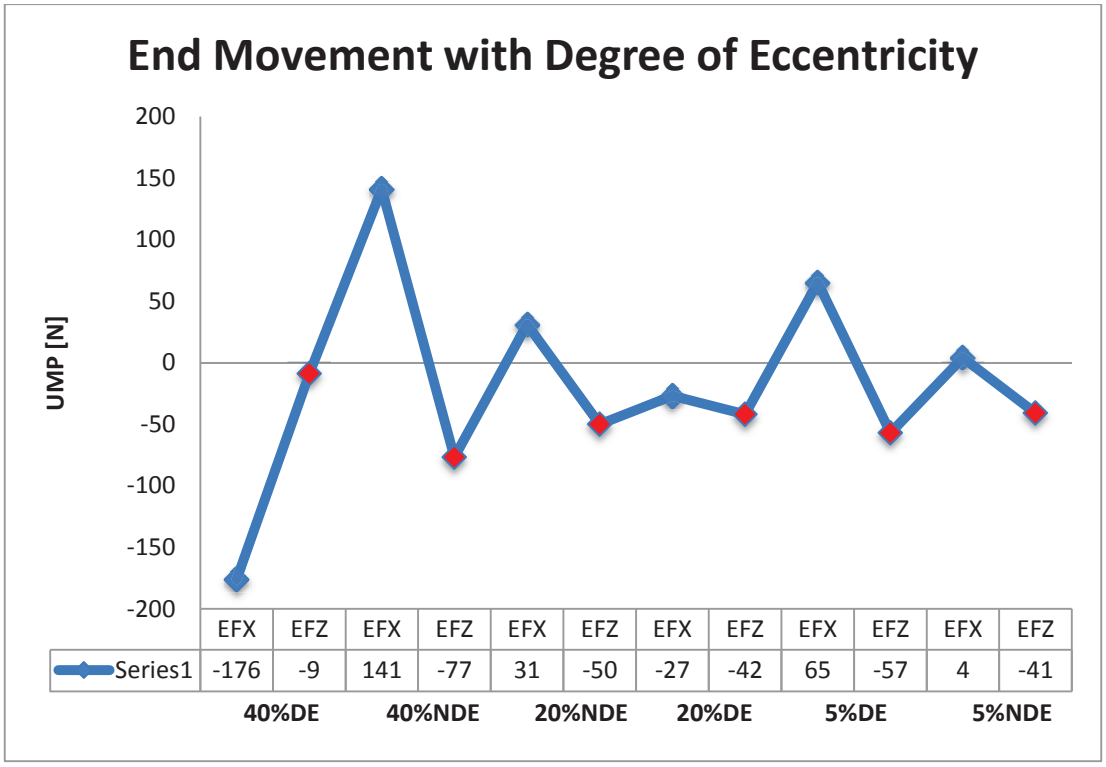

Figure 4.27: Comparison of UMP with different rotor eccentricities.

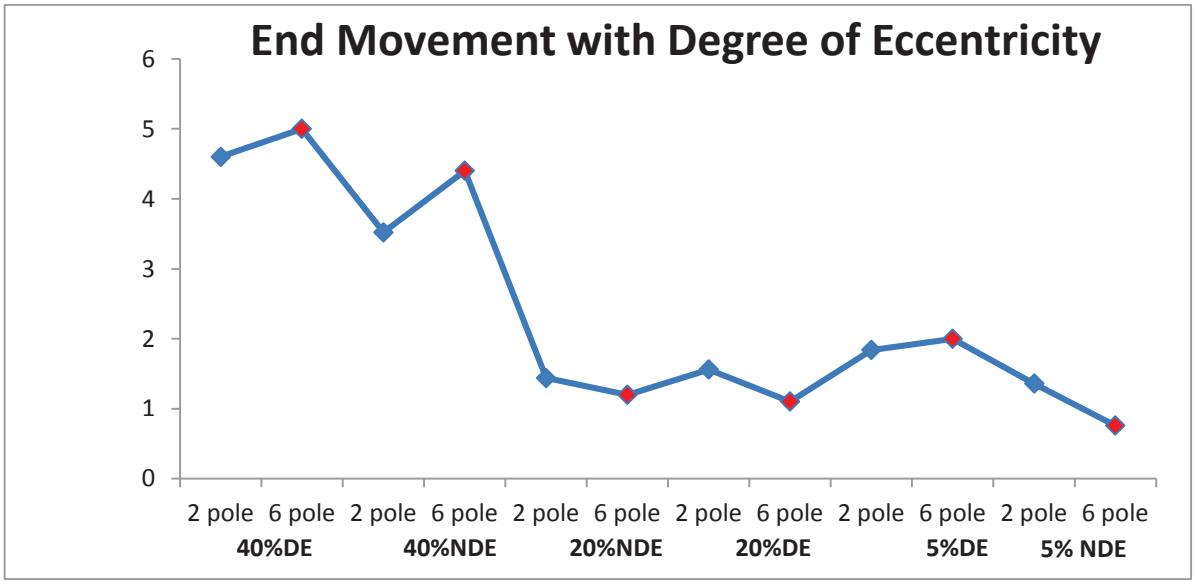

Figure 4.28: Comparison of voltage with different rotor eccentricities.

4.5. DC Testing

The test was performed by inducing DC into the 2- and 6-pole search coils in order to note the UMP. The search windings were supplied with 0.5 A current and the attenuation of UMP was tried to be noted. It showed a small change in the UMP and this was expected because the search coils have a low current rating and few turns. The induced current was of about correct rating of the wire used in search coils .This was not successful because the MMF is too low to make UMP attenuation effective. To produce additional Unbalanced Magnetic Pull, the windings need to have many more turns with ability to carry higher loading to be effective. For the above test, the induced voltages can be found using

$$V^{\alpha}_{pm-1,ph} = j\frac{3\pi\mu_0\omega L_{st}\bar{N}^1_{st}}{k^3 p_m\left(p_m-1\right)g_{av}}\bar{\delta}(\text{mean})\left(\bar{N}^{p_m-1}_{(SC-1)}\right)^*\bar{I}_{ph} \tag{4.19}$$

$$V^{\alpha}_{pm+1,ph} = \frac{3\pi\mu_0\omega L_{st}\bar{N}^1_{st}}{k^3 p_m\left(p_m+1\right)g_{av}}\bar{\delta}(\text{mean})\left(\bar{N}^{p_m+1}_{(SC+1)}\right)^*\bar{I}_{ph} \tag{4.20}$$

In the similar manner the equations for $V^{\beta}_{p_m-1,p_h}$ and $V^{\beta}_{p_m+1,p_h}$ can also be expressed.

Chapter 5: Conclusions and Future Work

This research work has developed techniques for measuring UMP in wound rotor induction machines and studied methods to reduce UMP. The results showed correlated with previous simulations of the machine. Open circuit and locked rotor conditions were implemented in order to achieve the results. These are standard tests for an induction machine.

From the experimental results, it is clearly indicated that the effect of UMP is affected by different rotor eccentricities, and with different axial variations of the eccentricity. The addition of 2- and 6-pole search windings also play a role in the detection and reduction of UMP. These search windings along with main windings were tested on different rotor eccentricities and the results proved successful in terms of detecting the eccentricity. Further work is needed to rewind the machine and test the damping capabilities of the damper windings. The voltages in the 2- and 6-pole specific windings were observed and were used to assess the rotor eccentricity. Here, the results were not successful because the search windings need an increase in the number of turns because the additional UMP damping can only be produced with more turns and the ability to carry higher loading.

Future work will be carried out using condition monitoring to control the UMP using impedance matrices. The impedance matrices will be programmed in Matlab and compared with the experimental results. The idea of using active voltage control for reduction of unbalanced magnetic pull will be also verified using the matrix:

$$\begin{bmatrix} v_{ph} \\ v^{\alpha}_{pm-1} \\ v^{\beta}_{pm-1} \\ v^{\alpha}_{pm+1} \\ v^{\beta}_{pm+1} \\ F_{\alpha} \\ F_{\beta} \end{bmatrix} = \begin{bmatrix} \bar{Z}_{ph,ph} & \bar{Z}^{\alpha}_{ph,pm-1} & \bar{Z}^{\beta}_{ph,pm-1} & \bar{Z}^{\alpha}_{ph,pm+1} & \bar{Z}^{\beta}_{ph,pm+1} \\ \bar{Z}^{\alpha}_{pm-1,ph} & \bar{Z}^{\alpha}_{ph,pm-1} & 0 & 0 & 0 \\ \bar{Z}^{\beta}_{pm-1,ph} & 0 & \bar{Z}^{\beta}_{ph,pm-1} & 0 & 0 \\ \bar{Z}^{\alpha}_{pm+1,ph} & 0 & 0 & \bar{Z}^{\alpha}_{ph,pm+1} & 0 \\ \bar{Z}^{\beta}_{pm+1,ph} & 0 & 0 & 0 & \bar{Z}^{\beta}_{ph,pm+1} \\ F_{\alpha,ph} & F^{\alpha}_{\alpha,pm-1} & F^{\beta}_{\alpha,pm-1} & F^{\alpha}_{\alpha,pm+1} & F^{\beta}_{\alpha,pm+1} \\ F_{\beta,ph} & F^{\alpha}_{\beta,pm-1} & F^{\beta}_{\beta,pm-1} & F^{\alpha}_{\beta,pm+1} & F^{\beta}_{\beta,pm+1} \end{bmatrix} \begin{bmatrix} i_{ph} \\ i^{\alpha}_{pm-1} \\ i^{\beta}_{pm-1} \\ i^{\alpha}_{pm+1} \\ i^{\beta}_{pm+1} \end{bmatrix} \tag{5.1}$$

This is the first stage of the impedance matrix development because it still assumes the rotor is open circuit. Rotor current inclusion is relatively straightforward.

Bibliography

1. Gray, A. and J. Pertsch Jr, *Critical Review of the Bibliography on Unbalanced Magnetic Pull in Dynamo-Electric Machines.* American Institute of Electrical Engineers, Transactions of the, 1918. **37**(2): p. 1417-1424.
2. Rosenberg, E., *Magnetic pull in electric machines.* Transactions of the american institute of electrical engineers, 1918. **2**(XXXVII): p. 1425-1469.
3. Robinson, R., *The calculation of unbalanced magnetic pull in synchronous and induction motors.* American Institute of Electrical Engineers, Transactions of the, 1943. **62**(10): p. 620-624.
4. Crawford, W., *Unbalanced magnetic pull and the mechanical stability of rotating electrical machines'.* Engineering, 1951. **171**: p. 504-505.
5. Covo, A., *Unbalanced magnetic pull in induction motors with eccentric rotors.* Transactions of the American Institute of Electrical Engineers. Part III: Power Apparatus and Systems, 1954. **2**(73): p. 1421-1425.
6. Summers, E.W., *Vibration in 2-pole induction motors related to slip frequency.* Transactions of the American Institute of Electrical Engineers. Part III: Power Apparatus and Systems, 1955. **3**(74): p. 69-72.
7. Robinson, R., *Line-frequency magnetic vibration of ac machines.* Power Apparatus and Systems, Part III. Transactions of the American Institute of Electrical Engineers, 1962. **81**(3): p. 675-679.
8. Jordan, H., G. Roder, and H. Weis, *Under what circumstances may mechanical vibrations of the stator core be expected at supply frequency in 4-pole, 3-phase asynchronous machines'.* ERA Translation IB2578, 1967. **21**(3): p. 91-95.
9. Rai, G., *Airgap eccentricity in induction motors*. 1974: ERA Technology Limited.
10. Ellison, A. and C. Moore. *Acoustic noise and vibration of rotating electric machines*. in *Proceedings of the Institution of Electrical Engineers*. 1968. IET.
11. Hellmund, R., *Series versus parallel windings for ac motors.* Electr. World, 1907. **49**: p. 388-389.
12. Krondl, M., *Self excited radial vibrations of the rotor of induction machines with parallel paths in the winding.* Bull. Assoc. Suisse Electr, 1956. **47**(1): p. 581-588.

13. Schuisky, W., *Magnetic pull in electrical machines due to the eccentricity of the rotor.* Electr. Res. Assoc. Trans, 1972. **295**: p. 391-399.

14. Binns, K. and M. Dye. *Identification of principal factors causing unbalanced magnetic pull in cage induction motors*. in *Proceedings of the Institution of Electrical Engineers*. 1973. IET.

15. Haasse, H., H. Jordan, and K.P. Kovacs, *Vibratratory forces as a result of shaft fluxes with two-pole induction machines.* Electrotech (ETZ), 1972. **93**: p. 458-486.

16. Kovacs, K., *Two-pole induction-motor vibrations caused by homopolar alternating fluxes.* Power Apparatus and Systems, IEEE Transactions on, 1977. **96**(4): p. 1105-1108.

17. Belmans, R., et al. *Unbalanced magnetic pull and homopolar flux in three phase induction motors with eccentric rotors*. in *Proceedings of International Conference on Electrical Machines*. 1982.

18. Belmans, R., et al. *Unbalanced magnetic pull in three phase two pole induction motors with eccentric rotor*. in *Proceedings of IEE-International Conference on Electrical Machines-Design and Applications*. 1982.

19. Belmans, R., A. Vandenput, and W. Geysen, *Calculation of the flux density and the unbalanced pull in two pole induction machines.* Electrical Engineering (Archiv fur Elektrotechnik), 1987. **70**(3): p. 151-161.

20. Yang, S. *Acoustic noise from small 2-pole single-phase induction machines*. in *Proceedings of the Institution of Electrical Engineers*. 1975. IET.

21. Timár-P, L.T.-P. and P. Tímár, *Noise and vibration of electrical machines*. Vol. 34. 1989: North Holland.

22. Zhu, Z. and D. Howe, *Effect of rotor eccentricity and magnetic circuit saturation on acoustic noise and vibration of single-phase induction motors.* Electric machines and power systems, 1997. **25**(5): p. 443-457.

23. Williamson, S., *Power-factor improvement in cage-rotor induction motors.* Electric Power Applications, IEE Proceedings B, 1983. **130**(2): p. 121-129.

24. Williamson, S. and A. Smith. *Steady-state analysis of 3-phase cage motors with rotor-bar and end-ring faults*. in *IEE Proceedings B (Electric Power Applications)*. 1982. IET.

25. Williamson, S. and K. Mirzoian, *Analysis of cage induction motors with stator winding faults.* IEEE Transactions on Power Apparatus and Systems, 1985. **7**(PAS-104): p. 1838-1842.

26. Williamson, S. and M. Abdel-Magied. *Steady-state analysis of double-cage induction motors with rotor-cage faults*. in *IEE Proceedings B (Electric Power Applications)*. 1987. IET.

27. Williamson, S. and N. Adams. *Cage induction motors with inter-rings*. in *IEE Proceedings B (Electric Power Applications)*. 1989. IET.

28. Swann, S. *Effect of rotor eccentricity on the magnetic field in the air-gap of a non-salient-pole machine*. in *Proceedings of the Institution of Electrical Engineers*. 1963. IET.

29. D. G. Dorrell and A. Smith, *Calculation of UMP in induction motors with series or parallel winding connections.* Energy Conversion, IEEE Transactions on, 1994. **9**(2): p. 304-310.

30. A. C. Smith and D.G. Dorrell, *Calculation and measurement of unbalanced magnetic pull in cage induction motors with eccentric rotors. Part 1: Analytical model.* IEE Proceedings-Electric Power Applications, 1996. **143**(3): p. 193-201.

31. Heller, B. and A. Jokl, *Tangential forces in squirrel-cage induction motors.* Power Apparatus and Systems, IEEE Transactions on, 1969(4): p. 484-492.

32. Vandevelde, L. and J. Melkebeek. *Theoretical and experimental study of radial forces in relation to magnetic noise of induction motors*. in *Proceedings of the International Conference on Electrical Machines (ICEM), 5-8 September Vol. 3*. 1994.

33. Früchtenicht, I.J. and I.H. Seinsch, *Exzentrizitätsfelder als Ursache von Laufinstabilitäten bei Asynchronmaschinen.* Archiv für Elektrotechnik, 1982. **65**(4-5): p. 271-281.

34. Stavrou, A. and J. Penman. *Modelling dynamic eccentricity in smooth air-gap induction machines*. in *Electric Machines and Drives Conference, 2001. IEMDC 2001. IEEE International*. 2001. IEEE.

35. Berman, M. *On the reduction of magnetic pull in induction motors with off-centre rotor*. in *Industry Applications Society Annual Meeting, 1993., Conference Record of the 1993 IEEE*. 1993. IEEE.

36. Toliyat, H. and T. Lipo, *Transient analysis of cage induction machines under stator, rotor bar and end ring faults.* Energy Conversion, IEEE Transactions on, 1995. **10**(2): p. 241-247.

37. Milimonfared, J., et al., *A novel approach for broken-rotor-bar detection in cage induction motors.* Industry Applications, IEEE Transactions on, 1999. **35**(5): p. 1000-1006.

38. Nandi, S. and H. Toliyat, *Novel frequency-domain-based technique to detect stator interturn faults in induction machines using stator-induced voltages after switch-off.* Industry Applications, IEEE Transactions on, 2002. **38**(1): p. 101-109.

39. Luo, X., et al., *Multiple coupled circuit modeling of induction machines.* Industry Applications, IEEE Transactions on, 1995. **31**(2): p. 311-318.

40. Lipo, T., *Theory and control of synchronous machines.* University of Wisconsin-Madison, 1987: p. ll.

41. Gojko, J.M., D.D. Momir, and O.B. Aleksandar, *Skew and linear rise of MMF across slot modelling-winding function approach.* Energy conversion, ieee transactions on, 1999. **14**(3): p. 315-320.

42. Al-Nuaim, N. and H. Toliyat. *A method for dynamic simulation and detection of dynamic air-gap eccentricity in synchronous machines*. in *Electric Machines and Drives Conference Record, 1997. IEEE International*. 1997. IEEE.

43. Al-Nuaim, N. and H. Toliyat, *A novel method for modeling dynamic air-gap eccentricity in synchronous machines based on modified winding function theory.* Energy Conversion, IEEE Transactions on, 1998. **13**(2): p. 156-162.

44. Nandi, S., et al. *Performance analysis of a three phase induction motor under mixed eccentricity condition*. in *Power Electronic Drives and Energy Systems for Industrial Growth, 1998. Proceedings. 1998 International Conference on*. 1998. IEEE.

45. Nandi, S., S. Ahmed, and H. Toliyat, *Detection of rotor slot and other eccentricity related harmonics in a three phase induction motor with different rotor cages.* Energy Conversion, IEEE Transactions on, 2001. **16**(3): p. 253-260.

46. Nandi, S., H. Toliyat, and A.G. Parlos. *Performance analysis of a single phase induction motor under eccentric conditions*. in *Industry Applications Conference, 1997. Thirty-Second IAS Annual Meeting, IAS'97., Conference Record of the 1997 IEEE*. 1997. IEEE.

47. Joksimovic, G.M., et al., *Dynamic simulation of dynamic eccentricity in induction machines-winding function approach.* Energy Conversion, IEEE Transactions on, 2000. **15**(2): p. 143-148.

48. Bossio, G., et al., *A 2-D model of the induction machine: an extension of the modified winding function approach.* Energy Conversion, IEEE Transactions on, 2004. **19**(1): p. 144-150.

49. Garrigan, N.R., et al. *Radial force characteristics of a switched reluctance machine*. in *Industry Applications Conference, 1999. Thirty-Fourth IAS Annual Meeting. Conference Record of the 1999 IEEE*. 1999. IEEE.

50. Dorrell, D., M. Ooshima, and A. Chiba. *Force analysis of a buried permanent-magnet bearingless motor*. in *Electric Machines and Drives Conference, 2003. IEMDC'03. IEEE International*. 2003. IEEE.

51. Li, J., Z. Liu, and L. Nay, *Effect of radial magnetic forces in permanent magnet motors with rotor eccentricity.* Magnetics, IEEE Transactions on, 2007. **43**(6): p. 2525-2527.

52. Dorrell, D. G., *The influence of rotor skew on unbalanced magnetic pull in cage induction motors with eccentric rotors.* 1995.

53. Dorrell, D.G., *Calculation of unbalanced magnetic pull in small cage induction motors with skewed rotors and dynamic rotor eccentricity.* Energy Conversion, IEEE Transactions on, 1996. **11**(3): p. 483-488.

54. Dorrell, D. G, *Experimental behaviour of unbalanced magnetic pull in 3-phase induction motors with eccentric rotors and the relationship with tooth saturation.* Energy Conversion, IEEE Transactions on, 1999. **14**(3): p. 304-309.

55. Dorrell, D. *Modelling of non-uniform rotor eccentricity and calculation of unbalanced magnetic pull in 3-phase cage induction motors*. in *International conference on electrical machines*. 2000.

56. Dorrell, D.G., et al., *Damper windings in induction machines for reduction of unbalanced magnetic pull and bearing wear.* Industry Applications, IEEE Transactions on, 2013. **49**(5): p. 2206-2216.

57. Wu, L., et al., *An analytical model of unbalanced magnetic force in fractional-slot surface-mounted permanent magnet machines.* Magnetics, IEEE Transactions on, 2010. **46**(7): p. 2686-2700.

58. Zhu, Z., et al., *Unbalanced magnetic forces in permanent-magnet brushless machines with diametrically asymmetric phase windings.* Industry Applications, IEEE Transactions on, 2007. **43**(6): p. 1544-1553.

59. Kelk, H.M., A. Eghbali, and H. Toliyat. *Modeling and analysis of cage induction motors under rotor misalignment and air gap eccentricity*. in *Industry Applications Conference, 2005. Fourtieth IAS Annual Meeting. Conference Record of the 2005*. 2005. IEEE.

60. Dorrell, D. and A. Smith, *Calculation and measurement of unbalanced magnetic pull in cage induction motors with eccentric rotors. Part 2: Experimental investigation.* IEE Proceedings-Electric Power Applications, 1996. **143**(3): p. 202-210.

61. Dorrell, D.G., A. Hermann, and B. Jensen. *Analysis of unbalanced magnetic pull in wound rotor induction machines using finite element analysis-Transient, motoring and generating modes*. in *Industrial Electronics Society, IECON 2013-39th Annual Conference of the IEEE*. 2013. IEEE.

62. Dorrell, D.G. and O. Kayani, *Measurement and Calculation of Unbalanced Magnetic Pull in Wound Rotor Induction Machine.* Magnetics, IEEE Transactions on, 2014. **50**(11): p. 1-4.

63. Ebrahimi, B.M. and J. Faiz, *Magnetic field and vibration monitoring in permanent magnet synchronous motors under eccentricity fault.* IET electric power applications, 2012. **6**(1): p. 35-45.

64. Wu, L., et al. *Eliminating load oscillation effects for rotor eccentricity detection in closed-loop drive-connected induction motors*. in *Power Electronics Specialists Conference, 2006. PESC'06. 37th IEEE*. 2006. IEEE.

65. Kim, D.-J., et al., *Estimation of acoustic noise and vibration in an induction machine considering rotor eccentricity.* Magnetics, IEEE Transactions on, 2014. **50**(2): p. 857-860.

66. Dorrell, D.G., *Sources and characteristics of unbalanced magnetic pull in three-phase cage induction motors with axial-varying rotor eccentricity.* Industry Applications, IEEE Transactions on, 2011. **47**(1): p. 12-24.

67. Chiba, A., T. Fukao, and M.A. Rahman, *Vibration suppression of a flexible shaft with a simplified bearingless induction motor drive.* Industry Applications, IEEE Transactions on, 2008. **44**(3): p. 745-752.

68. Sinervo, A., A. Laiho, and A. Arkkio, *Low-frequency oscillation in rotor vibration of a two-pole induction machine with extra four-pole stator winding.* Magnetics, IEEE Transactions on, 2011. **47**(9): p. 2292-2302.

69. Hwang, D.-H., et al., *Detection of air-gap eccentricity and broken-rotor bar conditions in a squirrel-cage induction motor using the radial flux sensor.* Journal of Applied Physics, 2008. **103**(7): p. 07F131.

70. Dorrell, D.G., W.T. Thomson, and S. Roach, *Analysis of airgap flux, current, and vibration signals as a function of the combination of static and dynamic airgap eccentricity in 3-phase induction motors.* Industry Applications, IEEE Transactions on, 1997. **33**(1): p. 24-34.

71. Thomson, W., D. Rankin, and D. Dorrell, *On-line current monitoring to diagnose airgap eccentricity in large three-phase induction motors-industrial case histories verify the predictions.* Energy Conversion, IEEE Transactions on, 1999. **14**(4): p. 1372-1378.

72. Ceban, A., R. Pusca, and R. Romary, *Study of rotor faults in induction motors using external magnetic field analysis.* Industrial Electronics, IEEE Transactions on, 2012. **59**(5): p. 2082-2093.

73. Verma, S.P. and R. Natarajan, *Effects of eccentricity in induction motors.* International Conference of Electric Machines, 1982: p. 930-933.

74. Frosini, L., et al. *Development of a leakage flux measurement system for condition monitoring of electrical drives*. in *Diagnostics for Electric Machines, Power Electronics & Drives (SDEMPED), 2011 IEEE International Symposium on*. 2011. IEEE.

75. Hwang, D.-H., et al. *A Method for Dynamic Simulation and Detection of Air-gap Eccentricity in Induction Motors by Measuring Flux Density*. in *Electromagnetic Field Computation, 2006 12th Biennial IEEE Conference on*. 2006. IEEE.

Appendix A: Motor Specifications

Name plate details	
Power [HP]	10 (or 7.46 kW)
Speed [rpm]	1420
Frequency [50]	50
Stator voltage [V]	400/440 Delta
Stator rated current [A]	13
Rotor Voltage [V]	200
Rated rotor current [A]	22
Poles	4
Slip [p.u.]	0.0533

Measured geometry [mm]	
Axial length Stator and Rotor cores	100.9 and 103.9
Stator outer and inner diameters	353 and 228.15
Rotor outer diameter	226.42
Shaft diameter	120
Airgap length	0.5
Stator and Rotor slots	48 and 36
Skew	1 rotor slot skew
Stator and Rotor Slot opening	3.9 and 3
Mean length of one Stator winding turn	847
Turns per slot	34 in series
Mean length of one Rotor winding turn	801.66
Stator and Rotor turns	48 and 72
Stator and Rotor wire diameter	1.725 and 1.9 – by calculation from SPEED
Stator winding	Single layer lap with 13 slot pitch
Stator Coil per pole per depth	2
Stator tooth width and length	8.22 and 26.82
Slot type	Round bottom, parallel tooth
Rotor tooth width and length	5.72 and 22.5
Slot type	Parallel slot, flat bottom
Slot width	3.5
Turns per coil	6 in series
Coils per phase	12
Rotor connection	Star through 3 slip rings
Rotor inertia	0.1734 kg/m^2
Stator and Rotor tooth tip depth	1 and 1

Measured resistances	
Rph stator (DC, cold)	1.82 ohm
Rph rotor (DC, cold)	0.23 ohm

Equivalent Circuit Parameters from SPEED	
R2’	3.01 ohm
X1	5.23 ohm
X2’	3.37 ohm
Xm (420 v line-line)	198 ohm
Rc (using M19 29 gage)	10 k ohm

Appendix B: 4 Pole Main Winding

This is one phase of the main 3-phase 4-pole winding.

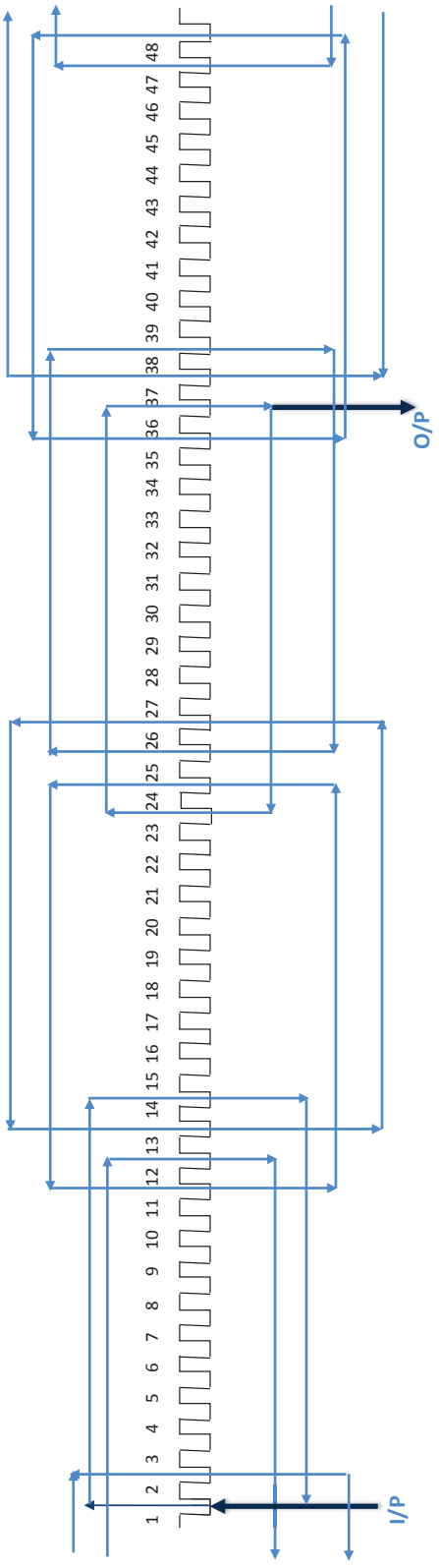

Appendix C: 2 Pole Search Windings

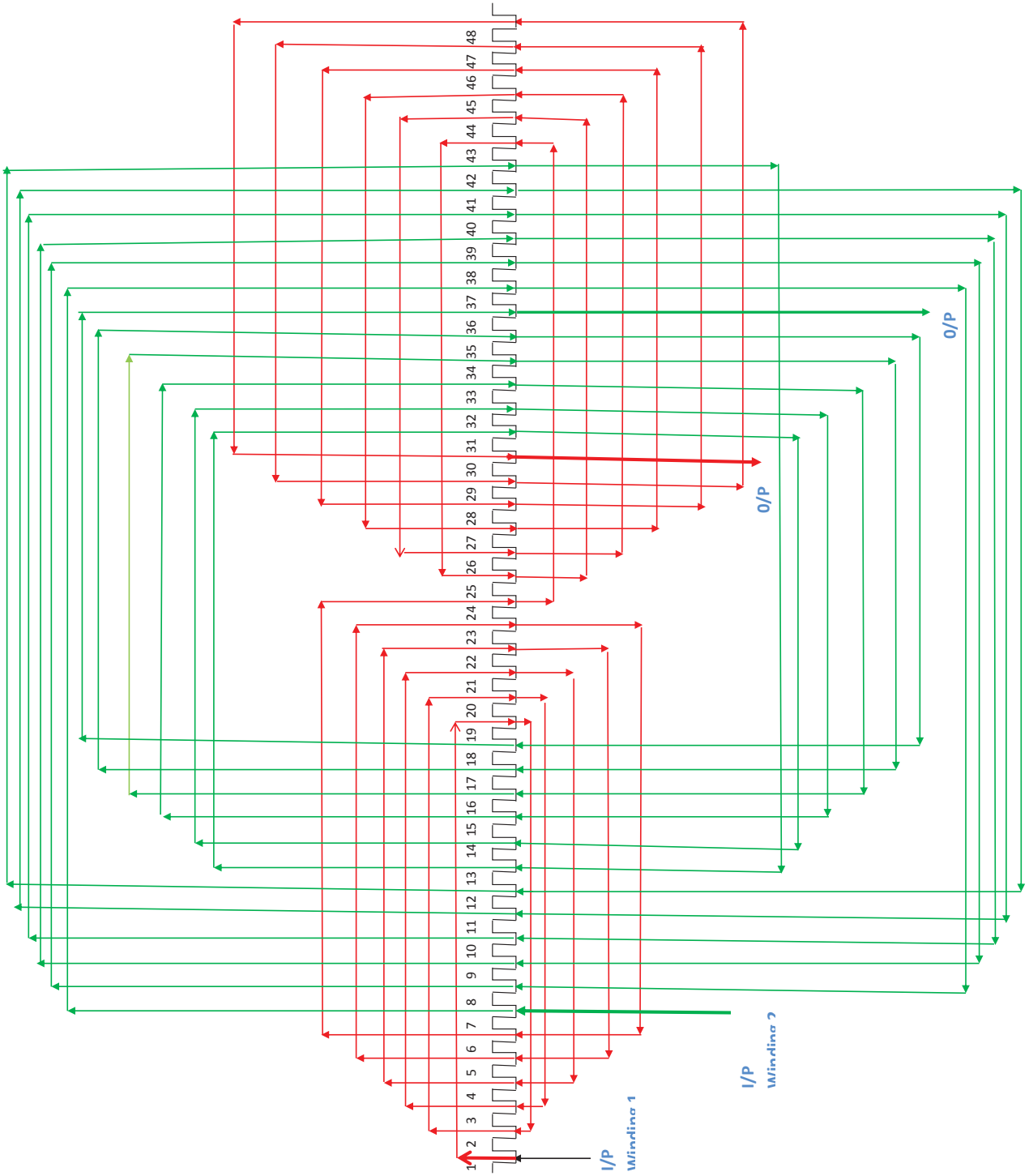

Appendix D: 6 Pole Search Winding

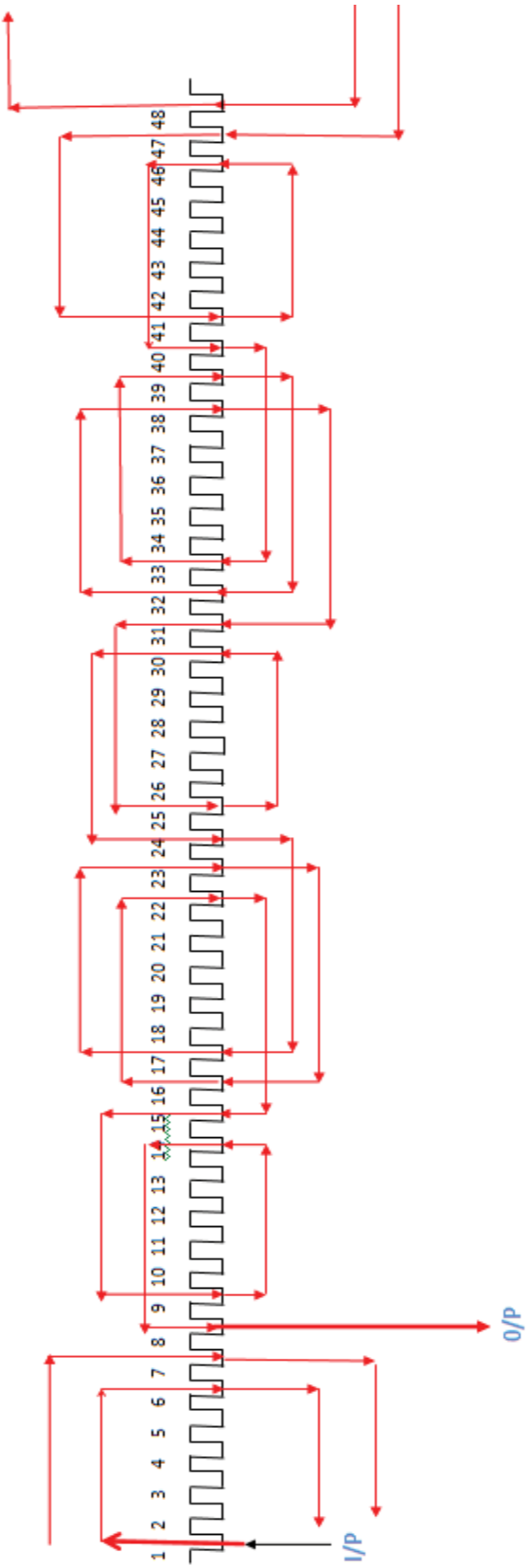

Appendix E: Power Connections

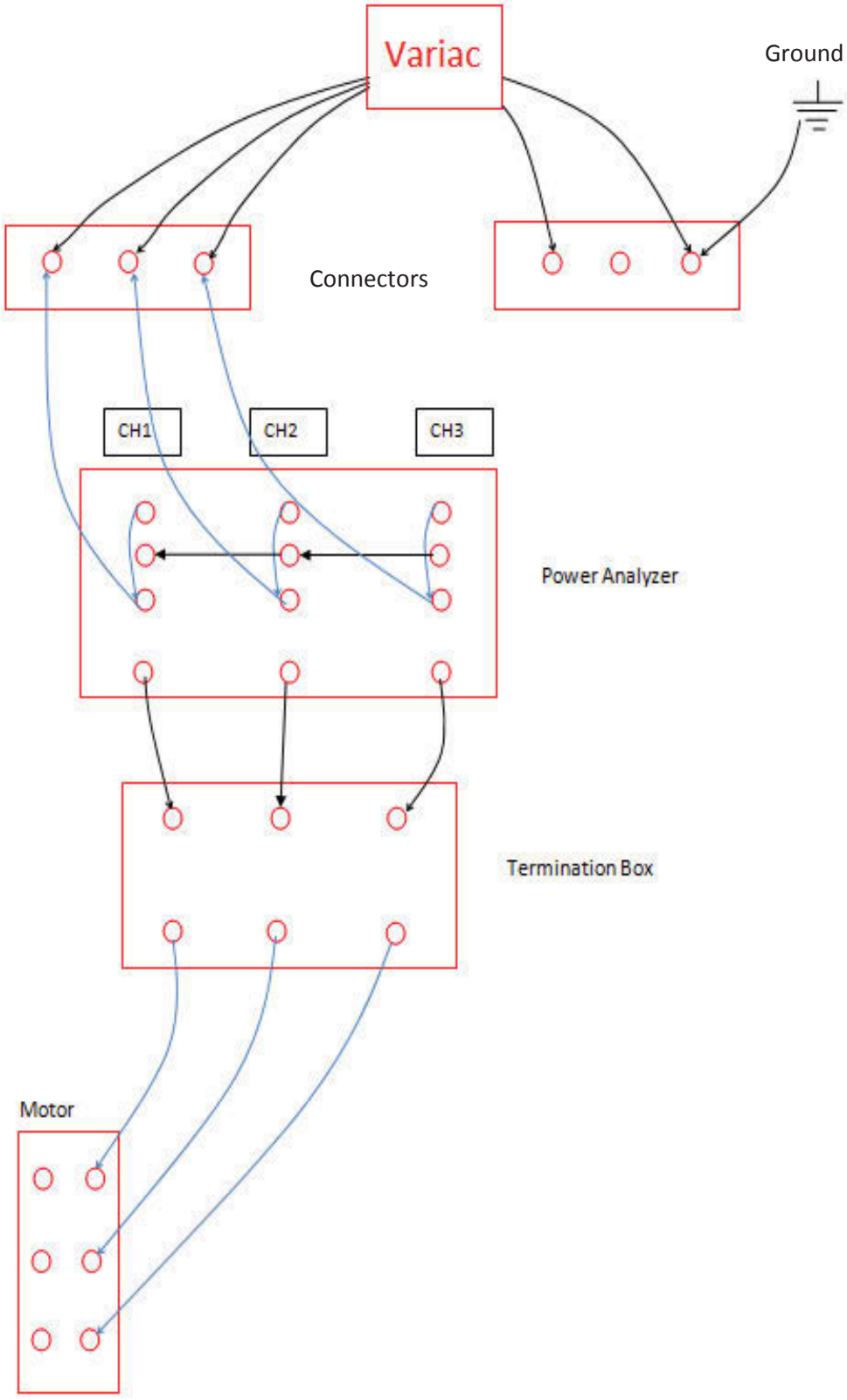

Appendix F: Technical Papers Published

The following papers have been published:

1. D. G. Dorrell, and O. Kayani. "Measurement and Calculation of Unbalanced Magnetic Pull in Wound Rotor Induction Machine." *Trans. on Magnetics, IEEE* Vol. 50, no. 11, Nov. 2014

2. D. G. Dorrell, O. Kayani and A. Salah, "The detection and suppression of Unbalanced Magnetic Pull in Wound Rotor Induction Motors Using Pole-Specific Search Coils and Auxiliary Windings," to be presented at *IEEE ECCE Conference*, Montreal, Sept 2015.